Article

Structure

Mechanism of CcdA-Mediated Rejuvenation of DNA Gyrase

Graphical Abstract

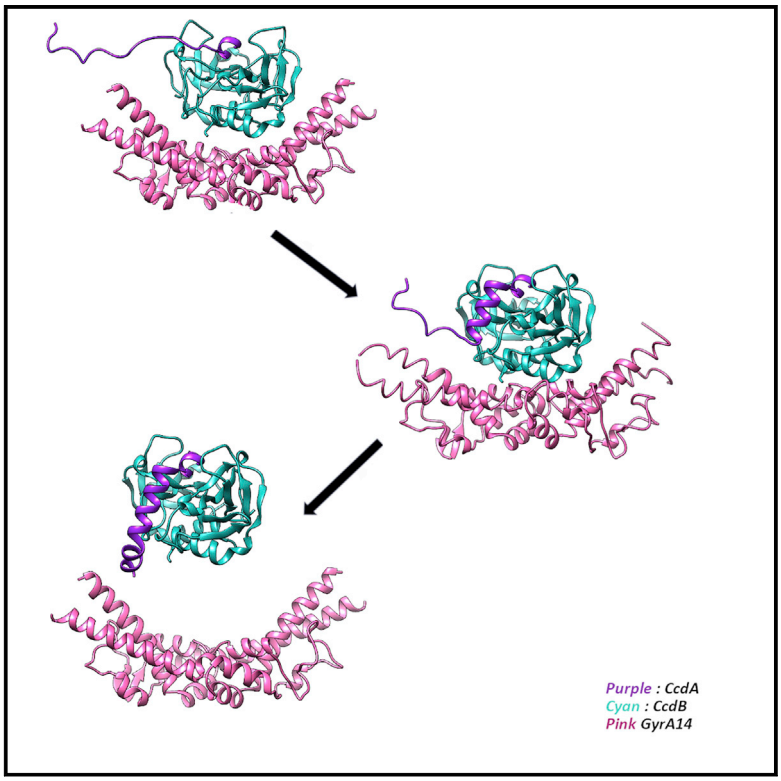

Authors

Nilesh K. Aghera, Jyothi Prabha, Himani Tandon, Gopinath Chattopadhyay, Sneha Vishwanath, Narayanaswamy Srinivasan, Raghavan Varadarajan

Correspondence

varadar@iisc.ac.in

In Brief

Aghera et al. elucidate the molecular mechanisms responsible for extraction of the bacterial toxin CcdB from its complex with DNA gyrase, using a combination of experimental FRET kinetic measurements and computational normal mode and perturbation response scanning analyses to identify and characterize the transient molecular complexes involved in the process.

Highlights

- CcdA antitoxin rejuvenates bacterial DNA gyrase by extracting bound CcdB toxin
- CcdA forms transient ternary and quaternary complexes with gyrase:CcdB complex
- Molecular basis for rejuvenation elucidated through computation and experiment
- Similar methodology can be used to characterize other transient complexes

Aghera et al., 2020, Structure *28*, 562–572
May 5, 2020
https://doi.org/10.1016/j.str.2020.03.006

CellPress

CellPress

Structure

Article

Mechanism of CcdA-Mediated Rejuvenation of DNA Gyrase

Nilesh K. Aghera,[1,3] Jyothi Prabha,[1,4] Himani Tandon,[1,4] Gopinath Chattopadhyay,[1] Sneha Vishwanath,[1] Narayanaswamy Srinivasan,[1] and Raghavan Varadarajan[1,2,5,*]

[1]Molecular Biophysics Unit, Indian Institute of Science, Bangalore 560 012, India

[2]Jawaharlal Nehru Centre for Advanced Scientific Research, Jakkur P.O., Bangalore 560 004, India

[3]Present address: National Center for Biological Sciences, Tata Institute of Fundamental Research, Bangalore 560 065, India

[4]These authors contributed equally

[5]Lead Contact

*Correspondence: varadar@iisc.ac.in

https://doi.org/10.1016/j.str.2020.03.006

SUMMARY

Most biological processes involve formation of transient complexes where binding of a ligand allosterically modulates function. The ccd toxin-antitoxin system is involved in plasmid maintenance and bacterial persistence. The CcdA antitoxin accelerates dissociation of CcdB from its complex with DNA gyrase, binds and neutralizes CcdB, but the mechanistic details are unclear. Using a series of experimental and computational approaches, we demonstrate the formation of transient ternary and quaternary CcdA:CcdB:gyrase complexes and delineate the molecular steps involved in the rejuvenation process. Binding of region 61–72 of CcdA to CcdB induces the vital structural and dynamic changes required to facilitate dissociation from gyrase, region 50–60 enhances the dissociation process through additional allosteric effects, and segment 37–49 prevents gyrase rebinding. This study provides insights into molecular mechanisms responsible for recovery of CcdB-poisoned cells from a persister-like state. Similar methodology can be used to characterize other important transient, macromolecular complexes.

INTRODUCTION

Toxin-antitoxin (TA) systems in bacteria are selfish elements, which ensure their own integrity and propagation during each cell division (Bernard and Couturier, 1992; Gerdes et al., 1986; Hayes, 2003; Pandey and Gerdes, 2005; Ramisetty and Santhosh, 2017). In addition to ensuring their own existence, they also equip the bacterial cells with certain survival advantages. Chromosomal TA systems are believed to restrict large-scale chromosomal alterations, but allow small alterations important for evolution, thereby ensuring balance between chromosomal stability and evolution (Christensen-Dalsgaard and Gerdes, 2006; Rowe-Magnus et al., 2003; Szekeres et al., 2007).

TA systems are classified into six different categories (types I–VI) based on the mode of function or the molecular nature of the toxin and antitoxin components (Chan et al., 2016). The ccd operon on the F plasmid of *E. coli* encodes a type II TA system, where the functional components of the system are proteins (Bernard and Couturier, 1992). The ccd operon is involved both in plasmid maintenance and bacterial drug tolerance (Bernard and Couturier, 1992; Gupta et al., 2017; Tripathi et al., 2012). The downstream ccdB gene of the ccd TA system encodes the toxin CcdB (homodimer) that mediates its toxicity by binding and inhibiting the function of homodimeric DNA gyrase (Bernard and Couturier, 1992). The toxicity of CcdB is inhibited by binding to the homodimeric CcdA encoded by the upstream ccdA gene (Bernard and Couturier, 1991, 1992; De Jonge et al., 2009; Madl et al., 2006). CcdA consists of DNA binding (residues 1–36) and CcdB binding (residues 37–72) domains. Contacts between CcdA and CcdB are largely in the 50–72-residue stretch of CcdA (De Jonge et al., 2009), which does not contact the GyrA binding site on CcdB. The intrinsically disordered C-terminal domain of CcdA acquires an ordered helical structure upon binding to CcdB (Figure 1). The N-terminal DNA binding domain of CcdA regulates expression of its own operon (Afif et al., 2001; Madl et al., 2006; Salmon et al., 1994). Under normal physiological conditions, the ccd operon expresses CcdA and CcdB, which bind to each other to form a non-toxic complex that auto-represses its own promoter. The half-life of the antitoxin is significantly lower due to its higher protease susceptibility compared with the toxin (Gerdes and Maisonneuve, 2012; Muthuramalingam et al., 2016; Van Melderen et al., 1994). Therefore, when the cell loses F plasmid or experiences proteolytic stress, CcdA will be depleted faster than CcdB, leading to growth inhibition or cell death (Gerdes and Maisonneuve, 2012; Gerdes et al., 1986; Tripathi et al., 2012, 2014). Growth can resume once cells experience favorable conditions by a mechanism that is still elusive (Kaspy et al., 2013; Maisonneuve et al., 2011; Page and Peti, 2016; Wood, 2016). Previous *in vitro* studies have shown that CcdA, in addition to inhibiting the toxicity of the CcdB, can also rejuvenate the poisoned gyrase by actively facilitating dissociation of the CcdB-gyrase complex (De Jonge et al., 2009; Maki et al., 1996). It is likely that the same functional ability of the antitoxin reverses growth inhibition *in vivo*. Since the CcdAB system has been shown to play a role in bacterial drug tolerance (Gupta et al., 2017; Tripathi et al., 2012), understanding the mechanism

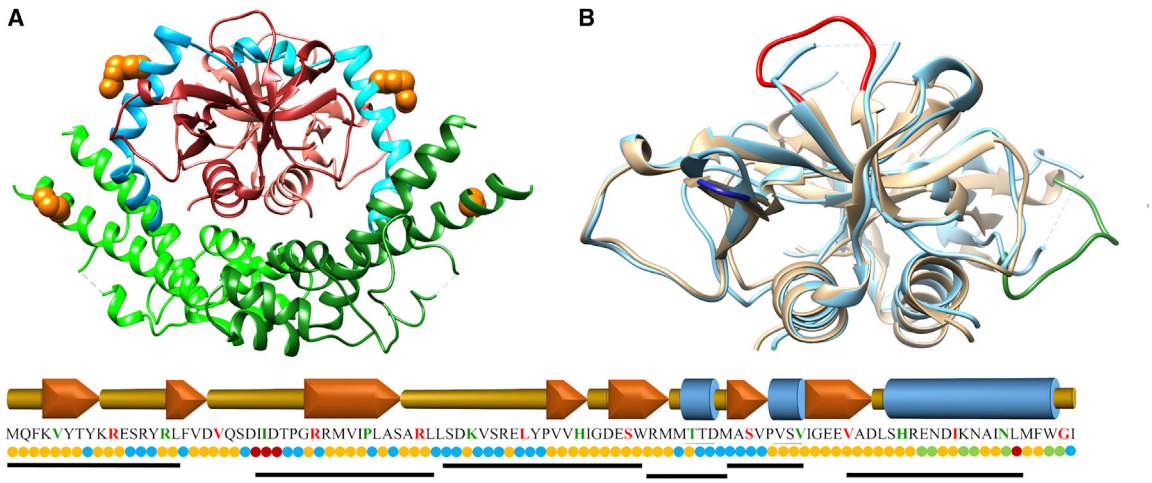

Figure 1. Structure of CcdB in Complex with its Binding Partners, CcdA and GyrA14

(A) Superposition of the CcdA-CcdB complex structure with the CcdB-GyrA14 complex to highlight the relative binding positions of the CcdA (blue) and GyrA14 (green) on CcdB (red). The structure was generated by aligning the CcdB homodimer from PDB: 3G7Z and 1X75. The CcdB structure bound to GyrA14 is not shown to improve the clarity. The two residues selected for FRET, namely CcdA-R57 and GyrA14-E487, are shown as orange spheres.

(B) Comparison of the conformations of CcdB bound to CcdA and GyrA14. The molecule shown in light cyan color represents the conformation of CcdB bound to GyrA14, whereas the wheat color represents the conformation of CcdB bound to CcdA. Backbones of both forms of CcdB are similar (RMSD = 1.1 Å) with the only noticeable difference in the region spanning from beta strand 1 to 2 (blue) and ordering of the loop regions from 10 to 15 (red) and 42 to 47 (green) upon CcdA binding. The loop movements could not have arisen due to crystal packing interactions because the CcdB loop regions that are ordered in both the CcdA complexes but disordered in the GyrA14 complex are not involved in crystal contacts, with the exception of CcdB residue E11. In addition, the CcdB 10-15 loop region has very similar conformations in both the CcdA-bound and free conformations, confirming that its conformation is not impacted by crystal contacts. One-dimensional view of the secondary structure of CcdB aligned to its amino acid sequence is shown below (A) and (B) In the sequence, every fifth and tenth residue was marked using green and red color, respectively. Below the sequence of CcdB, cyan, green, and dark red-colored spheres mark the residues, which bind to CcdA, GyrA14, and both, respectively. The yellow-colored spheres indicate residues that do not interact with either CcdA or GyrA14. Molecular graphics in (A) and (B) were made with the UCSF Chimera package (supported by NIGMS P41-GM103311) (Pettersen et al., 2004) (see also Tables S1–S4).

of gyrase rejuvenation may provide useful insights into mechanisms responsible for recovery of cells from a persister-like state.

CcdA and GyrA bind at partially overlapping sites on CcdB (Figure 1). The observation that the rate of dissociation of the CcdB-gyrase complex is significantly faster in the presence of CcdA as compared with its spontaneous dissociation rate, suggests that the process is actively catalyzed by CcdA through the formation of a ternary complex (De Jonge et al., 2009). However, the existence of the proposed ternary complex involving CcdA-CcdB-gyrase has not been experimentally confirmed so far. It is thus crucial to validate its existence to understand the molecular details of the rejuvenation process mediated by CcdA. It has been argued that binding of CcdA to CcdB modulates its structure, which facilitates the dissociation of gyrase (De Jonge et al., 2009), but comparative structural analysis of CcdB dimer in the free form (Loris et al., 1999), bound to CcdA peptide (De Jonge et al., 2009), and bound to GyrA14 (Dao-Thi et al., 2005) demonstrates that binding of either ligand does not cause large conformational changes (Figure 1B). This observation suggests the possibility that the rejuvenation process of gyrase is driven by dynamic alterations that precede the minor conformational changes.

In this study, we used the GyrA14 variant of gyrase (Dao-Thi et al., 2005) and three variants of CcdA ($CcdA_{36-72}$, $CcdA_{50-72}$, and $CcdA_{61-72}$), which contain the necessary binding domains that mediate dissociation of the CcdB-GyrA14 complex. We experimentally demonstrate for the first time, the existence of a short-lived transient ternary complex CcdA-CcdB-GyrA14 using fluorescence resonance energy transfer (FRET). The ternary complex so formed, eventually falls apart to yield the CcdA-CcdB complex and functional GyrA14 in the free form. The dissociation is enhanced by binding of a second molecule of CcdA to the ternary complex. Furthermore, normal mode analysis (NMA) studies suggest that, although binding of CcdA or GyrA14 to CcdB induces similar global dynamics in CcdB, there are subtle yet important changes at local sites in CcdB that facilitate the formation of the ternary complex. A segmental binding model was proposed based on available crystal structure data (De Jonge et al., 2009) where it was suggested that the CcdA segment from 61 to 72 binds to the CcdB-GyrA14 complex first, followed by the rest of CcdA. The present work refines and extends this model. Perturbation response scanning (PRS) studies suggest that CcdA induces changes in CcdB regions 8–12, 24–26, 67–72, and 80–96 to facilitate dissociation of CcdB from poisoned gyrase, and most of the perturbations in CcdB arise upon binding of the sequence segment 61–72 of CcdA. The remaining regions of CcdA induce further perturbations in CcdB upon binding, which appears to provide additional energy that favors CcdA binding over GyrA14.

RESULTS

Residue Selection for Designing the FRET Pairs to Monitor the Rejuvenation Process

A model of the CcdA-CcdB-GyrA ternary complex was generated (Figure 1) by superimposing crystal structure two

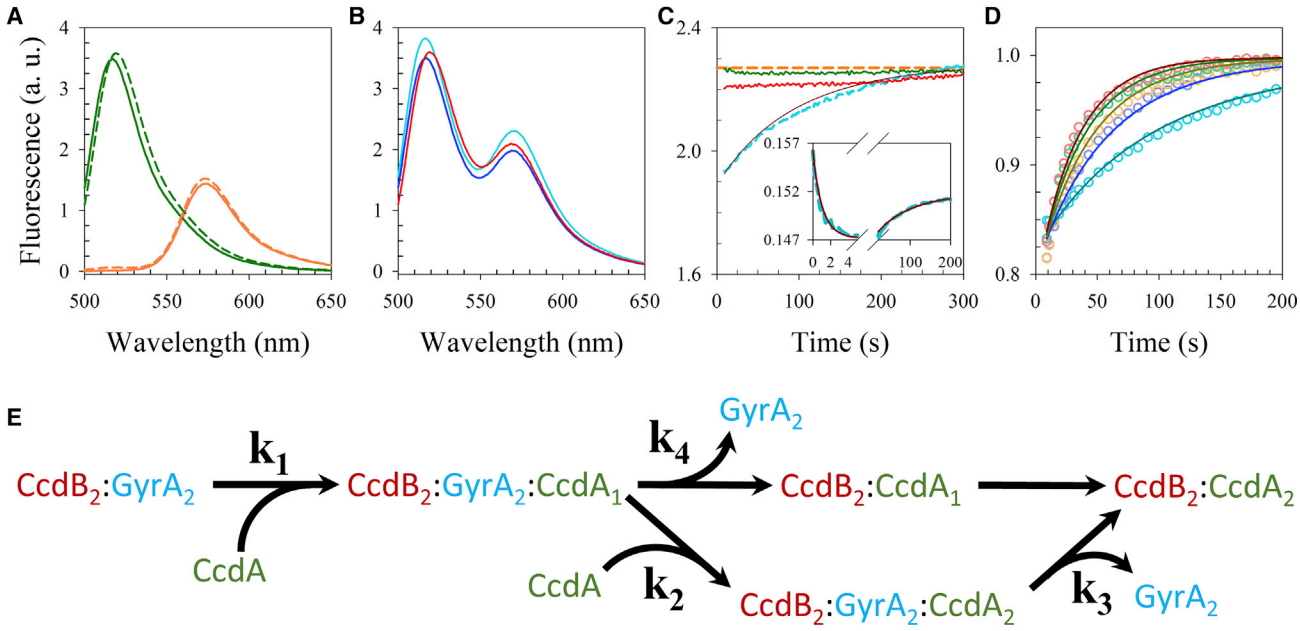

Figure 2. Transient Ternary Complex Captured Using FRET

(A) Spectral characterization of TMR-labeled CcdA (orange lines) and fluorescein-labeled GyrA14 (green lines) in the free form (solid lines) and in complex with CcdB (dashed lines).

(B) The arithmetic sum of TMR-labeled CcdA and fluorescein-labeled GyrA14 fluorescence spectra (solid blue line) coincides with the fluorescence spectrum obtained upon mixing them in the same solution with (solid red line) and without CcdB (solid cyan line). The fluorescence spectra in (A) and (B) were obtained using an excitation wavelength of 490 nm.

(C) Temporal changes in the donor fluorescence observed when a preformed complex of CcdB-GyrA14* was mixed with either $CcdA_{50\text{-}72}$* (dashed cyan line) or with unlabeled CcdA (solid green line). The solid red line represents the fluorescence change upon mixing a preformed complex of CcdB-$CcdA_{50\text{-}72}$* with GyrA14*. The solid brown line represents the fit through the data using the kinetic scheme shown below, whereas the dashed orange line marks the expected equilibrium signal for the donor fluorophore. Inset shows a representative stopped-flow monitored kinetic trace (dashed cyan line) and fit through the data (solid brown line) using the kinetic scheme.

(D) Concentration dependence of the rejuvenation process. Time-dependent change in fluorescence observed upon mixing 1 μM of a preformed complex of CcdB-GyrA14* with $CcdA_{50\text{-}72}$* at final concentrations of 1 μM (cyan circle), 2 μM (blue circle), 3 μM (yellow circle), 4 μM (green circle), and 5 μM (red circle). The solid lines in respective colors show global fit to the data using the kinetic scheme.

(E) Kinetic scheme that describes the rejuvenation process. The k_i values indicate the forward rate constants for the various reactions. The rate constants for the reverse reactions (k_{-i}) are not shown for ease of visualization. $K_i = k_i/k_{-i}$ is the equilibrium constant for reaction i (see also Figures S3–S5).

complexes, namely CcdB:GyrA (1X75) and CcdB:CcdA (3G7Z), using UCSF Chimera software (Pettersen et al., 2004). Two residues in this model were selected, one from CcdA (R57) and the other from GyrA (E487), in such a way that they obey the following three constraints: (1) the Cα-Cα distances of the selected residues (27.6 Å) lie within the Förster distance (Ro value = 51 Å); (2) they are not at the binding interface; and (3) they are exposed with accessibility >20%. Residue accessibilities and interfacial residues were identified using PREDBURASA (Bommakanti et al., 2010). The corresponding wild-type (WT) amino acids were modified to cysteine and labeled with maleimide-conjugated fluorophores through cysteine chemistry. The FRET pair is designed such that FRET can occur only when CcdA interacts transiently with a preformed CcdB-GyrA complex. Thus, FRET can be used to monitor complex formation.

Rejuvenation Is a Concentration-Dependent, Biphasic Process

The $CcdA_{50\text{-}72}$ peptide was used for the FRET-monitored rejuvenation studies, as it facilitates the dissociation of the CcdB-GyrA14 complex as efficiently as $CcdA_{36\text{-}72}$ and the $CcdA_{50\text{-}72}$ and GyrA binding sites on CcdB are non-overlapping. The $CcdA_{50\text{-}72}$ and GyrA14 were labeled (denoted by *) with tetramethylrhodamine (acceptor) and fluorescein (donor), respectively. The ability of the labeled proteins to bind CcdB was verified before undertaking FRET studies. The fluorescence spectra of the labeled fluorophores of $CcdA_{50\text{-}72}$* and GyrA14* are identical to the fluorescence spectra of the CcdB-$CcdA_{50\text{-}72}$* complex and CcdB-GyrA14* complex (Figure 2A), respectively. Furthermore, the fluorescence spectrum obtained upon mixing $CcdA_{50\text{-}72}$* and GyrA14* in an equimolar ratio is identical to the sum of the individually obtained fluorescence spectra of $CcdA_{50\text{-}72}$* and GyrA14* (Figure 2B) as they do not interact with each other. The steady-state fluorescence spectrum obtained upon mixing CcdB, $CcdA_{50\text{-}72}$*, and GyrA14* is also expectedly identical to that of the sum of the individually obtained fluorescence spectra of $CcdA_{50\text{-}72}$* and GyrA14* as this results from the CcdB-$CcdA_{50\text{-}72}$* complex and free GyrA14* (Figure 2B).

The rejuvenation process was initiated by mixing the GyrA14*-CcdB complex with $CcdA_{50\text{-}72}$* and tracked by monitoring the change in donor (fluorescein) fluorescence on GyrA14. $CcdA_{50\text{-}72}$

was used for the FRET-monitored rejuvenation studies, as it facilitates the dissociation of the CcdB-GyrA14 complex as efficiently as $CcdA_{36-72}$ (data not shown) and harbors most of the CcdB binding residues that do not overlap with GyrA14 binding residues. The process was studied using stopped-flow and by manual mixing. The stopped-flow monitored process starts with a fast decrease in donor fluorescence that occurs over 5 s (Figure 2C). The fast decrease in fluorescence is followed by a slow increase in fluorescence that occurs over 200 s (Figure 2C). The fast decrease in the donor fluorescence is due to FRET, which occurs upon binding of $CcdA_{50-72}$* to the CcdB-GyrA14* complex, while the slow increase in donor fluorescence arises from the dissociation of the GyrA14*. As collected stopped-flow data are consistent with the manual mixing experiment, they were also used in the analysis. None of the interpretations derived in the study is solely based on the stopped-flow data. In manual mixing studies, the dead time of mixing was 10 s, therefore, only the slow phase corresponding to the increase in the donor fluorescence could be captured (Figure 2C). The donor fluorescence does not change when rejuvenation studies were carried out using unlabeled CcdA (Figure 2C). In addition, no change in donor fluorescence was observed when GyrA14* was added to the preformed CcdB-$CcdA_{50-72}$* complex as $CcdA_{50-72}$ has a higher affinity for CcdB than GyrA14. The concentration dependence of the rejuvenation kinetics is much lower than anticipated for a second-order reaction. This suggests that CcdA binding is not the rate-limiting step (Figure 2D).

NMA Suggests Subtle Dynamic Alterations in CcdB on Ligand Binding

A low root-mean-square deviation (RMSD) between CcdB structures taken from CcdA-bound (PDB: 3HPW) and GyrA14-bound (PDB: 1X75) forms suggests that the conformational change in CcdB is subtle (Figure 1B). CcdA and gyrase bind to CcdB on complementary regions (Figure 1A), where CcdA has 29 and gyrase has 7 unique interacting residues on CcdB (Tables S1–S4). Only four residues (24, 25, 26, and 96) on CcdB interact with both CcdA and GyrA14. Interestingly, the intra-molecular polar interactions of CcdB are significantly different in the CcdA-bound state compared with the GyrA14-bound state, suggesting a rearrangement of contacts. To probe the dynamics of free CcdB dimer and the CcdB dimer bound to either CcdA or gyrase, normal modes for CcdB in three forms were calculated using ANM-NMA. NMA suggests that the flexibility of CcdB residues that interact with CcdA is different among the three forms (blue boxed region in Figure 3). Interestingly, binding of GyrA14 alters the dynamics of CcdB residues interacting with CcdA but not those involved in interaction with GyrA14 (yellow boxed region in Figure 3). In the modeled ternary complex, CcdA residues 61–72 show no steric overlap with GyrA or CcdB residues. Regions 67–72 and 8–12 of CcdB interact with the incoming $CcdA_{61-72}$. CcdB region 67–72 shows low flexibility in all the three forms of CcdB (Figure 3), implying its importance in binding to CcdA and hints at possible significance of this region in the rejuvenation process. Residues that interact with both CcdA and GyrA14 (24–26) also show subtle differences in fluctuations in the three forms of CcdB (green boxed region in Figure 3).

PRS Analysis Points to Residues Important for the Rejuvenation Process

To identify CcdA binding residues on CcdB that are important in the rejuvenation process, PRS was performed for the CcdB-GyrA14 complex. PRS analysis identifies two sets of residues, namely effectors and sensors, which are important for allosteric communication within a protein (Dutta et al., 2015; General et al., 2014). The most effective residues (effectors) are the ones that cause maximum perturbation in structure, and the most sensitive residues (sensors) are the ones that are maximally perturbed. The effectiveness of perturbations at all CcdB residues, is presented in Figure 4A. Key effectors identified are residues 1–5, 50–53, 20–25, 32–34, 65–71, and 88–100 (Figure 4A). These regions on CcdB harbor either CcdA binding or gyrase binding sites (Tables S1–S4) (Dao-Thi et al., 2005; De Jonge et al., 2009). The most sensitive sensors correspond to the terminal residues on GyrA14, but other sensors on CcdB are residues 9–13, 40–44, 57–60, and 77–81 (Figure 4B).

The response to perturbation was analyzed as a three-step process to mimic the binding of CcdA to the CcdB-GyrA14 complex in three segments, namely $CcdA_{61-72}$, $CcdA_{50-60}$, and $CcdA_{37-49}$. The effectiveness and sensitivity profiles were used to understand the transmission of molecular signal from the $CcdA_{61-72}$ binding site to the GyrA14 binding site (primarily CcdB residues 98–101 and 24–26). From the effectiveness profile (Figure 4A), it was observed that CcdB region 65–71 is effective in causing perturbations in the CcdB-GyrA14 complex. Since this region harbors $CcdA_{61-72}$ binding residues (67, 69, 71, and 72), their effectiveness profiles were individually plotted in Figures 5A–5D. These residues were found to be effective in perturbing spatially proximal regions along with a few distant residues. A strong effect was observed on the residue stretch 9–13, which also forms part of the $CcdA_{61-72}$ binding region, and region 41–45, which binds to the next segment of CcdA ($CcdA_{50-60}$). Although the signal from these residues cannot directly propagate to the C-terminal site that forms the primary GyrA14 binding site (CcdB residues 98–100), its strong effect on the $CcdA_{50-60}$ binding site (CcdB residues 41–45) and a weak impact on another GyrA14 binding site (24–26) may be important in triggering rejuvenation.

CcdB residues I24, I25, and D26 are known to interact with both CcdA and GyrA14. Hence, it is important for CcdA to disrupt their interactions with GyrA14 to facilitate a stable CcdA complex with CcdB. Because CcdB residues 24–26 are not the most sensitive residues, their coupling to the $CcdA_{61-72}$ binding region was explored by individually plotting their sensitivity profiles (Figures 6 and 7). It was observed that, apart from neighboring residues, I24, I25, and D26 are influenced by perturbation in CcdB regions 65–72 and 40–55.

The next proposed event is the binding of segment 50–60 of CcdA ($CcdA_{50-60}$). These interactions are mediated by regions 40–55 and 24–26 of CcdB. As discussed above, binding of $CcdA_{61-72}$ impacts motion of 24–26 and 40–55 segments of CcdB, which possibly weakens its interaction with GyrA. The sensitivity profiles of residues W99 (Figure 7) and G100 also show their response to perturbations at I24, I25, and D26. Binding of $CcdA_{50-60}$ to the above residues causes further changes in CcdB conformation, leading to dissociation of GyrA from the ternary complex. In all the PRS analyses, since a unit

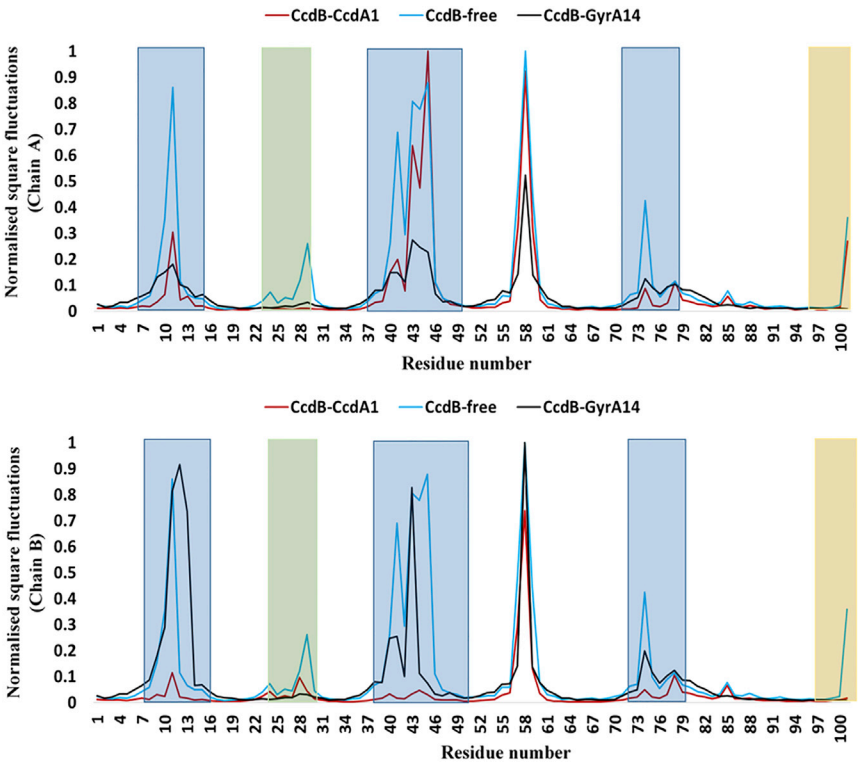

Figure 3. Flexibility Profile of CcdB in the Three Forms

The normalized square fluctuations obtained for CcdB in CcdA-bound (red), GyrA14-bound (black), and free (blue) for chain A (top) and chain B (bottom). Residues known to bind CcdA, GyrA14, or both are boxed in blue, yellow, and green, respectively. While free CcdB forms a symmetric homodimer, symmetry is lost in both the GyrA14- and CcdA-bound crystal structures.

force is applied at each residue position and the response is averaged over 1,000 applications in random directions, the different plots can only be qualitatively compared.

To probe the effect of including a larger GyrA fragment on the dynamics of the CcdB:GyrA complex, a homology model was generated using a larger GyrA fragment from *B. subtilis* (PDB: 4DDQ) in combination with the *E. coli* CcdB:GyrA14 complex structure (PDB: 1X75). A PRS study with this modeled complex yielded results similar to that obtained with the CcdB:GyrA14 complex. Since the latter is derived from an actual crystal structure rather than a homology model, we have focused only on those results here.

S12G Mutation Retards the Rejuvenation Process Mediated by CcdA

CcdB residues 8–14 are involved in binding $CcdA_{61-72}$, which is likely the initial stage of ternary complex formation. Residue S12 in CcdB contacts the terminal D71 residue in CcdA. Both WT CcdB and S12G-CcdB bind GyrA14 to similar extents in the absence of CcdA. This is expected since S12G is far from the gyrase binding site. When CcdA was passed over the CcdB-GyrA14 complex, dissociation of CcdB was observed, and the rate of dissociation increased with increasing CcdA concentration (Figure S1). The dissociation rate of CcdB was significantly slower (~5-fold) for the S12G variant of CcdB relative to that of the WT. Furthermore, the identical K_D values of WT and S12G CcdB with CcdA indicate that the affinity of CcdB for CcdA has remained unaffected by the S12G mutation (Figure S2). The observation that the rate of rejuvenation of CcdB by WT CcdA monitored using SPR (Figure S1) is similar to the rate of rejuvenation observed in FRET studies (Figure 2) confirms that the presence of fluorophores on the GyrA and CcdA proteins does not affect the rejuvenation process and further validates the kinetic mechanism and parameters inferred from the FRET studies.

DISCUSSION

Molecular switches play a central role in many regulatory mechanisms, where binding of one or more ligands to a target protein brings about desired functional changes through allosteric effects (Schreiber, 2017). CcdA is one such molecular switch that restores gyrase function by facilitating extraction of CcdB from its complex with GyrA14. The conformational state of the disordered C-terminal domain of CcdA regulates its recognition by Lon protease, and is also involved in binding to CcdB (Burger et al., 2017; Drobnak et al., 2013; Madl et al., 2006). Binding of CcdA to CcdB inhibits CcdB toxicity as well as autoregulating transcription of the ccd operon (De Jonge et al., 2009). An important role for the 61–72 region of CcdA in mediating rejuvenation was previously proposed based on structural (X-ray) and kinetic (SPR) studies. A transient ternary CcdA:CcdB:gyrase complex was inferred to be present but could not be experimentally detected (De Jonge et al., 2009). The previous descriptions of allostery are purely based on structural comparison of CcdB in the CcdA- and GyrA14-bound forms. Despite a low RMSD between the two CcdB structures, a rigid body shift, leading to rearrangement at the dimer interface of CcdB was observed. Further, the flipping of W99 and ordering of loop residues 7–12 of CcdB has also been reported (De Jonge et al., 2009). Although a comparison of static structures identifies some of the important conformational changes, a better understanding of how the signal is transmitted within the CcdB molecule leading to flipping of the W99 side chain is important in filling the gaps. Further, consistent with current views of allostery, it is equally important to understand the role of dynamics in mediating the dissociation. The present study provides experimental validation of the transient ternary complex, identifies a novel quaternary complex, and describes details of the molecular mechanisms responsible for rejuvenation using kinetic studies probed by FRET, in combination with data from NMA and PRS studies. The results from NMA and PRS analyses presented in this study complement the structural analyses of allostery.

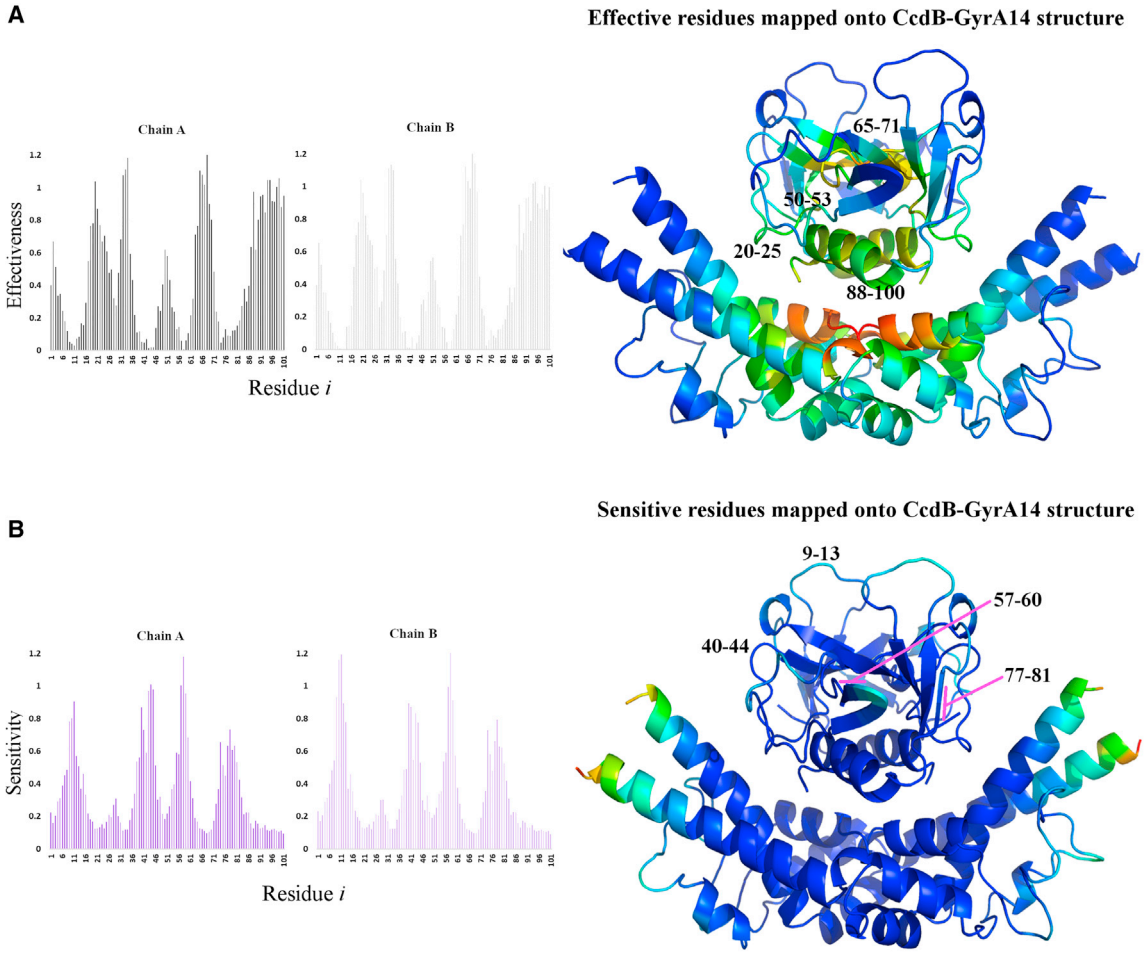

Figure 4. Perturbation Response Scanning Analysis

(A) Mean effectiveness of each CcdB residue (in chain A and chain B) is shown as bar plot on the left. The height of the bar is proportional to the average effect of perturbation at residue *i*, on the CcdB-GyrA14 complex. Values for the two chains of CcdB are shown in black and gray respectively. The average effectiveness of each residue is mapped onto the CcdB-GyrA14 structure on the right. Red to blue color indicates highest to lowest effect of perturbing residue *i*. The most effective residues span various regions, including regions 67–72, 20–25, and 50–53, which are known to bind the segments $CcdA_{61-72}$ and $CcdA_{50-60}$, respectively, and residues 88–100 involved in GyrA binding. These regions are marked on the CcdB structure.

(B) Mean sensitivity of individual residues is shown as a bar plot on the left. The height of the bar is proportional to the average response of each residue to perturbations at other sites. Two chains of CcdB are shown in dark purple and light purple, respectively. The average sensitivity of all residues is mapped onto the CcdB-GyrA14 structure on the right. Decreasing sensitivity is colored from red to blue. The sensitive residues include regions 9–13 and 40–44, which are likely to change conformation after binding to $CcdA_{61-72}$ and $CcdA_{50-60}$, respectively. These regions are marked on the CcdB-GyrA14 structure

See also Figures S1 and S2.

Rejuvenation Proceeds through Ternary and Quaternary Complexes

To obtain quantitative insights into the rejuvenation mechanism, FRET kinetic data as a function of CcdA concentration were globally fit to various models. The simplest mechanism that may operate during the rejuvenation process is shown in the kinetic scheme in Figure 2E, where one molecule of CcdA binds to the $CcdB_2$-$GyrA14_2$ complex. This transient complex may have two fates; it can dissociate to yield the CcdA-$CcdB_2$ complex and GyrA14 dimer or alternatively it can bind to a second molecule of CcdA and then dissociate into a $CcdA_2$-$CcdB_2$ complex and GyrA14 dimer. It should be noted that all the CcdA peptides used in this study are monomeric, whereas full-length CcdA forms a homodimer. However, only one protomer from the $CcdA_2$ homodimer can bind to $CcdB_2$. Another protomer from a second $CcdA_2$ homodimer binds to $CcdB_2$ at a partially overlapping site albeit with lower affinity (De Jonge et al., 2009). Thus, in the present studies, the binding of a single peptide to CcdB is equivalent to binding of a single CcdA dimer to the CcdB dimer, with all the interfacial residues being contributed by a single CcdA monomer of the dimer.

To further delineate the mechanism of rejuvenation, the scheme was globally fit to all the kinetic data. If the data were fit assuming that the dissociation of GyrA14 requires binding of two CcdA molecules and binding of a single CcdA cannot facilitate the rejuvenation of gyrase ($\lambda_4 << \lambda_3$), then the fits were not good (Figure S3A). Alternatively, if it

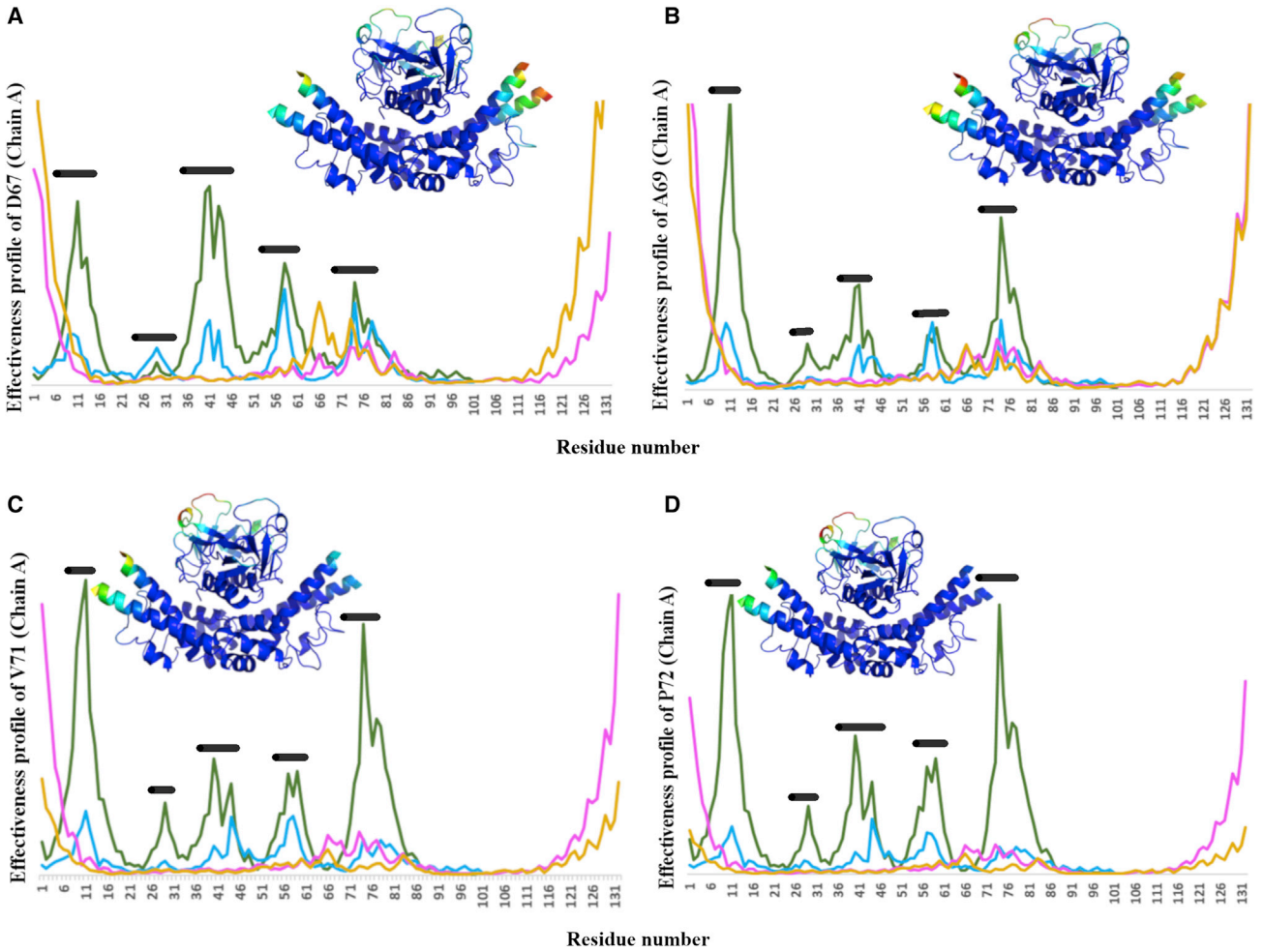

Figure 5. Effectiveness Profile of CcdB Residues Known to Interact with $CcdA_{61-72}$

Individual effectiveness profiles of CcdB residues (A) D67, (B) A69, (C) V71, and (D) P72 from chain A on all other residues of the CcdB-GyrA14 complex are plotted as line graphs. Different chains of the complex are colored as green (chain A of CcdB), blue (chain B of CcdB), pink (chain A of GyrA14), and yellow (chain B of GyrA14). Black horizontal lines depict residues that are most affected by perturbations at $CcdA_{61-72}$ binding residues. These regions include residues 8–16, 36–46, 55–60, and 70–80 in both subunits of CcdB. A small peak can also be observed at region 24–30 involved in both GyrA and CcdA binding. The effectiveness profiles mapped onto the CcdB-GyrA14 structure are presented in the inset (see also Figures S1 and S2).

was assumed that the binding of a second CcdA molecule is very slow as compared with the dissociation facilitated by a single CcdA molecule ($\lambda_2 << \lambda_4$), the scheme still failed to fit the data (Figure S3B). However, when data were fitted using the entire scheme without any constraint, the obtained fits were satisfactory, including fit to the stopped-flow data (Figures 2C and 2D. These results suggest that rejuvenation proceeds through pathways involving both ternary ($CcdB_2$:$GyrA_2$:CcdA) and quaternary ($CcdB_2$:$GyrA_2$:$CcdA_2$) complexes. The parameters obtained suggest that the rate of the dissociation of gyrase is faster in the presence of two protomers of CcdA peptide compared with that in the presence of a single CcdA (Table 1).

The inferred mechanism was further corroborated by an additional experiment. From the parameters listed in Table 1, it is evident that the rejuvenation facilitated by the binding of a single chain of CcdA is much slower than that catalyzed by the binding of two chains of CcdA. This observation was tested by performing the rejuvenation of the CcdB-GyrA14 complex using a CcdA concentration, half that of CcdB. Under such a condition, the lower affinity for binding of the second CcdA molecule would favor binding of a single CcdA molecule to each molecular complex of $CcdB_2$-$GyrA14_2$. Thus predominantly, the slow pathway of rejuvenation would be operational. The rejuvenation process shows a 5-fold reduction in the rate when carried out using the same concentration of the $CcdB_2$-$GyrA14_2$ complex but using half of the concentration of CcdA (Figure S4). This dramatic reduction in the rejuvenation rate indicates that rejuvenation is now operating only through the slow pathway. This result further confirms that there are two pathways of rejuvenation facilitated by the binding of a single and two molecules of CcdA, respectively, which differ in their kinetics. Previous studies have reported that the rejuvenation can be facilitated by the binding of a single CcdA molecule based on equilibrium endpoint studies (De Jonge et al., 2009); however, the present report provides

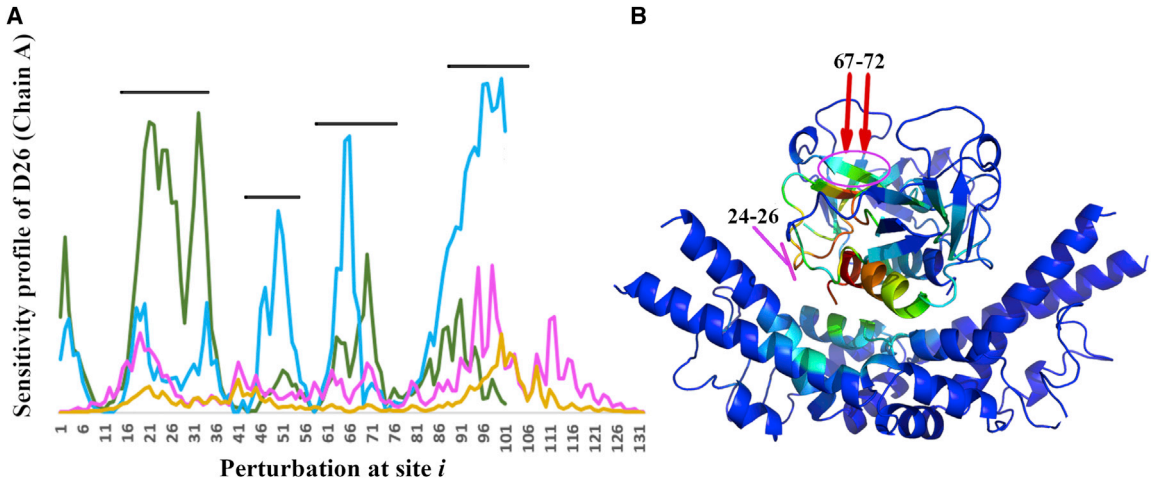

Figure 6. Sensitivity Profile of One of the Residues Involved in Binding Both GyrA14 and CcdA

Sensitivity of D26 on chain A to perturbation at all the other sites on the CcdB-GyrA14 complex.

(A) Different chains of the complex are colored as green (chain A of CcdB), blue (chain B of CcdB), pink (chain A of GyrA14), and yellow (chain B of GyrA14). The peaks (marked by horizontal lines) correspond to the residues which have the highest influence on D26. Apart from the neighboring residues, D26 is also sensitive to perturbation at 67–72 (brown horizontal line) and 45–55 (orange horizontal line) regions from both subunits of CcdB.

(B) The profile mapped onto the CcdB-GyrA14 structure. Warmer to cooler color indicate residues with highest to lowest effect on D26. Also marked in red and pink arrows are regions 67–72 and 24–26, respectively, on the CcdB-GyrA14 structure.

quantitative insights into rejuvenation through multiple pathways, and also clarifies the physiological significance of the low-affinity CcdA binding site on $CcdB_2$. While the present studies used fluorescein-labeled CcdA and GyrA derivatives, the fluorescence labels did not alter binding affinity and regeneration kinetics as analyzed by SPR and microscale thermophoresis studies (Figure S5).

Recognition of the CcdB-GyrA14 Complex by CcdA

Because the rejuvenation proceeds through formation of ternary and quaternary complexes, it is important to understand the features of CcdB that allow it to simultaneously bind to CcdA and gyrase but restrict its coexistence with both the proteins. Therefore, structural and dynamic studies were undertaken to probe CcdB in its free form, in complex with CcdA and in complex with GyrA14. It is not immediately obvious why a ternary complex involving $CcdA_{50\text{-}72}$, GyrA14, and CcdB is unstable since the binding sites on CcdB for $CcdA_{50\text{-}72}$ and GyrA14 are non-overlapping. However, in an *in silico* model ternary complex of $CcdA_{50\text{-}72}$:CcdB:GyrA, generated by superposing the known CcdA:CcdB and CcdB:GyrA structures, there is a steric clash between the side chains of residues 50–55 from the $CcdA_{50\text{-}70}$ segment and residues 45–47 from one subunit of CcdB. Hence, the side-chain conformations need to be modulated to allow $CcdA_{50\text{-}72}$ binding. Similarly, an attempt to generate a ternary complex of GyrA14 with the CcdB-$CcdA_{36\text{-}72}$ complex leads to steric clash between the GyrA14 and CcdA backbones, especially in the CcdA region 37–50. CcdA and GyrA14 have distinct interactions with sequence segments 69–75 and 80–96 of CcdB, but these regions show similar flexibility in NMA profiles in CcdA- and GyrA14-bound forms (Figure 3). Possibly the similarity in structural form and dynamics of CcdB in complex with GyrA14 and CcdA is important for the recognition of its binding site on the CcdB-GyrA14 complex by CcdA.

Early Events of CcdA Binding

The N-terminal domain (residues 1–36) of CcdA binds to DNA and regulates the expression of its own operon and the C-terminal intrinsically disordered domain (residues 37–72) binds to CcdB and regulates its toxicity. Because the N-terminal domain of CcdA has no role to play in the regulation of the toxicity of CcdB (Dao-Thi et al., 2005; De Jonge et al., 2009), and the $CcdA_{61\text{-}72}$ peptide achieves approximately 30% rejuvenation under the conditions used in this study, as compared with the longer peptides which cause complete rejuvenation (manuscript in preparation), all the studies were carried out using the C-terminal region of CcdA spanning residues 36–72. Most of the CcdB interface is present in $CcdA_{50\text{-}72}$ except for residues that bind CcdB residues 24, 47, 49, 96, and 101. The binding sites of $CcdA_{50\text{-}72}$ and $CcdA_{61\text{-}72}$ on CcdB do not overlap with the GyrA binding site except for residue 25 and 26, which make contact with residue 52 of $CcdA_{50\text{-}72}$, yet both these peptides can also trigger GyrA dissociation from CcdB (Figure 2) (De Jonge et al., 2009). This suggests that the C-terminal dodecapeptide of CcdA ($CcdA_{61\text{-}72}$), which binds to CcdB regions 8–14 and 67–72, is sufficient to induce most but not all the conformational and dynamic changes in CcdB. Importantly, PRS shows that binding of $CcdA_{61\text{-}72}$ in region 67–72 of CcdB is a crucial event, as these residues on CcdB are among the effectors that cause changes in motions throughout the molecule, including small changes in motions of CcdB residues 24–26 at the CcdB-GyrA14 interface (Figures 4, 5, 6, and 7) as well. Since the $CcdA_{61\text{-}72}$ binding region is completely accessible in the gyrase-bound form, we propose that $CcdA_{61\text{-}72}$ makes initial interactions with the 67–72 and 8–12 sequence stretch, thereby inducing local yet pivotal changes in flexibility of CcdB, hence transitioning it to a CcdA-bound form. The importance of residue S12 in the rejuvenation process was

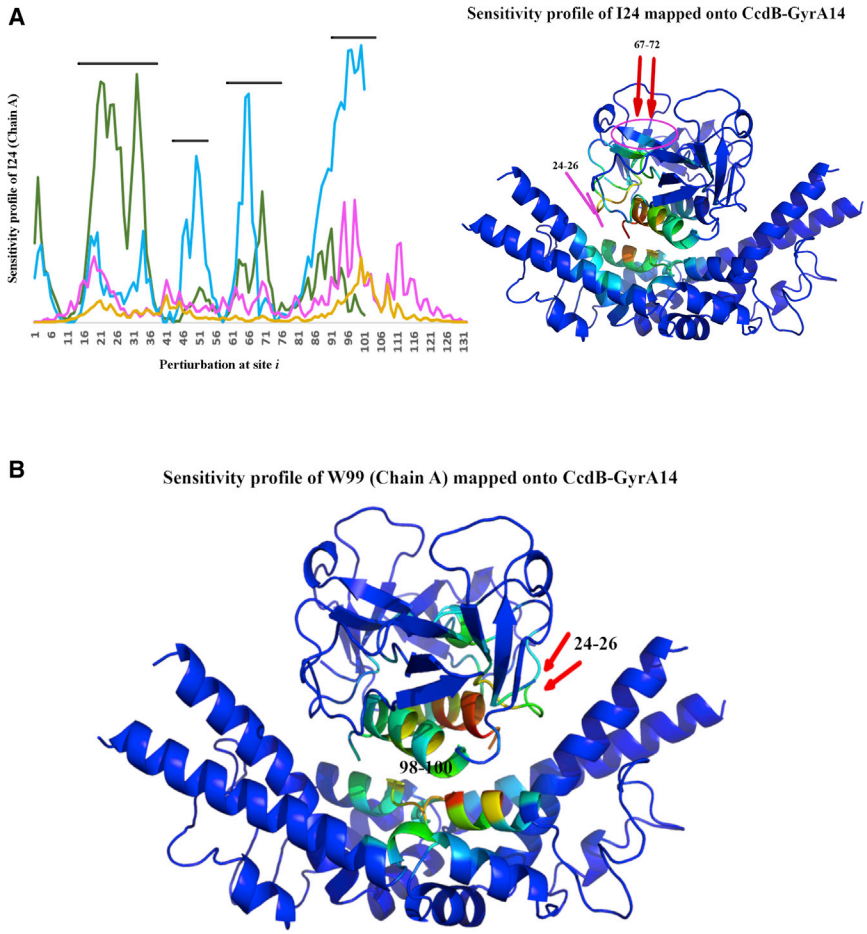

Figure 7. Sensitivity Profile of CcdB Residues I24 and W99

(A) Sensitivity of I24 (chain A) to perturbation at all the other sites on CcdB-GyrA14 complex. Different chains of the complex are colored as green (chain A of CcdB), blue (chain B of CcdB), pink (chain A of GyrA14), and yellow (chain B of GyrA14). The peaks (marked by black horizontal lines) correspond to the residues which have highest influence on I24. Apart from the neighboring residues, I25 and I26 are also sensitive to perturbation at 67–72 and 45–55 regions from both subunits of CcdB. The profile mapped onto the CcdB-GyrA14 structure is shown on the right. Warmer to cooler color indicate residues with highest to lowest effect on I24 and I25. Also marked in red and pink arrows are CcdB regions 67–72 and 24–26. I25 also shows a similar sensitivity profile.

(B) PRS sensitivity profile of residue W99 of CcdB (chain A) mapped onto the CcdB-GyrA14 structure. Warmer to cooler color indicate residues with high to low effect on W99. There exists a cross-communication between the two subunits such that W99 of one subunit is sensitive to I25 and D26 of the other subunit of CcdB (marked in red arrows). G100 also shows a similar sensitivity profile toward I25 and D26.

confirmed by the large decrease in rejuvenation kinetics seen in the S12G CcdB mutant. The intrinsically disordered nature of CcdA may play a crucial role in catalyzing rejuvenation as has been seen for other systems involving intrinsically disordered proteins (Berlow et al., 2017; Gruszka et al., 2016). Through NMA analysis, a few residues were identified that can mediate these subtle changes in CcdB when bound to GyrA14. These residues include Y8, F17, L36, L50, and I56 of CcdB. These residues may prove important in the information transfer.

The CcdB region 24–41, which hosts the common binding residues 24, 25, and 26, shows different dynamics in the GyrA14-bound and in the CcdA-bound form as seen by NMA (Figure 3). PRS studies suggest that residues I24, I25, and D26, which interact with both CcdA and gyrase, are sensitive to perturbations at CcdA binding residues (67–72) on CcdB involved in binding $CcdA_{61-72}$ (Figure 6). These observations suggest that binding to $CcdA_{61-72}$ facilitates loosening of the ternary complex. In support of this, we have previously shown (Tripathi et al., 2012) that perturbations to CcdB residue 24 decrease binding to GyrA but not to CcdA.

Late Binding Events

Although the binding of $CcdA_{61-72}$ is sufficient to rejuvenate CcdB-poisoned gyrase, it is not as efficient in displacing gyrase from CcdB as $CcdA_{36-72}$ (De Jonge et al., 2009). The binding of CcdA residues 50–60 appears to have an additional role in weakening the interactions between CcdB and gyrase by binding to residues 26–28, 37–46, and 64–66 of CcdB. PRS analysis revealed that perturbation of residues 24–26 on CcdB can affect the primary GyrA binding residue W99 (Figures 5 and 7). Thus, further binding of residues 50–60 of CcdA perturbs the gyrase

Table 1. Parameters for the Rejuvenation Process Described in the Kinetic Scheme

	First CcdA Binding	Second CcdA Binding	Dissociation of Hexameric Complex	Dissociation of Pentameric Complex
Forward rate constant	(k_1) 1.4 × 10^6 M^{-1} s^{-1}	(k_2) 1.1 × 10^5 M^{-1} s^{-1}	(k_3) 0.04 s^{-1}	(k_4) 0.0035 s^{-1}
Reverse rate constant	(k_{-1}) 0.003 s^{-1}	(k_{-2}) 0.19 s^{-1}	(k_{-3})[a] 2.2 M^{-1} s^{-1}	(k_{-4})[a] 2.2 M^{-1} s^{-1}
Equilibrium constant	(K_1) 5.8 × 10^8 M^{-1}	(K_2) 5.7 × 10^5 M^{-1}	(K_3)[a] 390 M	(K_4)[a] 261 M

Kinetic parameters were obtained by globally fitting rejuvenation kinetic traces to the scheme in Figure 2E.

[a]To determine the robustness of the parameters listed, fitting was initiated from various initial parameters. The values flagged with the superscript 'a' had standard deviations higher than their mean values. All other values were highly robust showing standard deviations of less than 50% for multiple independent fittings.

binding region. Finally, residues 40–49 contact residues 96 and 101 of CcdB preventing exposure of the key GyrA binding residue W99. Region 80–96 contains several GyrA14 binding residues. The binding of the first molecule of CcdA is followed by the binding of a second CcdA molecule. Although the binding affinity of the second CcdA is lower due to the asymmetric nature of binding, we show above that it enhances the dissociation rate of gyrase form CcdB by ~10-fold (Video S1).

In summary, this study clearly demonstrates that CcdA binds to CcdB-GyrA14 to form short-lived transient ternary and quaternary complexes of GyrA14, CcdB, and CcdA. While such short-lived complexes are involved in several regulatory processes, due to their transient nature, very few studies have characterized these processes in molecular detail (Berlow et al., 2017; Kamar et al., 2017; Li et al., 2017). The binding of the sequence segment 61–72 of CcdA to CcdB induces all the vital structural and dynamic changes required to facilitate dissociation from gyrase, segment 50–60 enhances the dissociation process through additional allosteric effects, and segment 37–49 prevents gyrase rebinding.

STAR★METHODS

Detailed methods are provided in the online version of this paper and include the following:

- KEY RESOURCES TABLE
- LEAD CONTACT AND MATERIALS AVAILABILITY
- EXPERIMENTAL MODEL AND SUBJECT DETAILS
- METHOD DETAILS
  - Protein Expression, Purification and Labeling
  - Construction of Cysteine Mutants in Gyrase
  - Purification and Labeling of GyraseA14 Cysteine Mutants
  - Rejuvenation Kinetic Studies
  - Equilibrium and Kinetic Fluorescence Studies
  - Fluorescence Kinetic Data Analysis
  - Structural Analysis
  - Computational Analyses
  - Normal Mode Analysis (NMA)
  - Perturbation Response Scanning (PRS)
  - Sequence Conservation Analysis for CcdB
  - SPR Experiments
- QUANTIFICATION AND STATISTICAL ANALYSIS
- DATA AND CODE AVAILABILITY

SUPPLEMENTAL INFORMATION

Supplemental Information can be found online at https://doi.org/10.1016/j.str.2020.03.006.

ACKNOWLEDGMENTS

We thank Professor Jayant B. Udgaonkar, Indian Institute of Science Education and Research, Pune for use of stopped-flow setups. We thank the MBU Proteomic facility for use of mass spectrometers. R.V. and N.S. acknowledge the financial support received from the Department of Biotechnology (grant number no. BT/COE/34/SP15219/2015, DT.20/11/2015), Government of India. N.A. is DST-INSPIRE AORC fellow. H.T. is a DST-INSPIRE fellow. J.P. is ICMR fellow. This research is also supported by the Indian Institute of Science-DBT partnership program (to R.V. and N.S.) and Mathematical Biology program of Department of Science and Technology to N.S. N.S. and R.V are J.C. Bose National Fellows. Support for infrastructural facilities from Fund for Improvement of Science and Technology infrastructure (FIST), DST and Centre for Advanced Structures (CAS), University Grants Commission (UGC), and the Ministry of Human Resource Development (MHRD) is also acknowledged. We are thankful to Dr. Sivaramaiah Nallapeta, Head Business Operations, Nano Temper Technologies and Dr. Saji Menon, Application Specialist, Nano Temper Technologies for the nanoTycho and MST facility. The assistance of Nonavinakere Seetharam Srilatha is duly acknowledged for the SPR experiments.

This work was funded by the Department of Science and Technology (DST), Government of India and Department of Biotechnology (DBT), Government of India.

AUTHOR CONTRIBUTIONS

N.K.A., J.P., and G.C. designed the experiments, analyzed the experimental data and wrote the experimental sections. H.T. performed the computations and wrote the computational sections. H.T. and S.V. analyzed the computational data. N.S. and R.V. supervised the research and acquired the funding. All authors reviewed the manuscript.

DECLARATION OF INTERESTS

The authors declare no competing interests.

Received: September 13, 2019
Revised: February 17, 2020
Accepted: March 17, 2020
Published: April 14, 2020

SUPPORTING CITATIONS

The following references appear in the Supplemental Information: Tripathi et al., 2019 and Wienken et al., 2010.

REFERENCES

Afif, H., Allali, N., Couturier, M., and Van Melderen, L. (2001). The ratio between CcdA and CcdB modulates the transcriptional repression of the ccd poison-antidote system. Mol. Microbiol. *41*, 73–82.

Ashkenazy, H., Abadi, S., Martz, E., Chay, O., Mayrose, I., Pupko, T., and Ben-Tal, N. (2016). ConSurf 2016: an improved methodology to estimate and visualize evolutionary conservation in macromolecules. Nucleic Acids Res. *44*, W344–W350.

Bajaj, K., Chakrabarti, P., and Varadarajan, R. (2005). Mutagenesis-based definitions and probes of residue burial in proteins. Proc. Natl. Acad. Sci. U S A *102*, 16221–16226.

Bajaj, K., Dewan, P.C., Chakrabarti, P., Goswami, D., Barua, B., Baliga, C., and Varadarajan, R. (2008). Structural correlates of the temperature sensitive phenotype derived from saturation mutagenesis studies of CcdB. Biochemistry *47*, 12964–12973.

Bakan, A., Meireles, L.M., and Bahar, I. (2011). ProDy: protein dynamics inferred from theory and experiments. Bioinformatics *27*, 1575–1577.

Baliga, C., Varadarajan, R., and Aghera, N. (2016). Homodimeric *Escherichia coli* toxin CcdB (controller of cell division or death B protein) folds via parallel pathways. Biochemistry *55*, 6019–6031.

Berendsen, H.J.C., van der Spoel, D., and van Drunen, R. (1995). GROMACS: a message-passing parallel molecular dynamics implementation. Computer Phys. Commun. *91*, 43–56.

Berlow, R.B., Dyson, H.J., and Wright, P.E. (2017). Hypersensitive termination of the hypoxic response by a disordered protein switch. Nature *543*, 447–451.

Berman, H.M., Westbrook, J., Feng, Z., Gilliland, G., Bhat, T.N., Weissig, H., Shindyalov, I.N., and Bourne, P.E. (2000). The protein data bank. Nucleic Acids Res. *28*, 235–242.

Bernard, P., and Couturier, M. (1991). The 41 carboxy-terminal residues of the miniF plasmid CcdA protein are sufficient to antagonize the killer activity of the CcdB protein. Mol. Gen. Genet. *226*, 297–304.

Bernard, P., and Couturier, M. (1992). Cell killing by the F plasmid CcdB protein involves poisoning of DNA-topoisomerase II complexes. J. Mol. Biol. *226*, 735–745.

BIAevaluation Software Handbook version 3.0. (1997). BIAevaluation Software Handbook version 3.0 (Uppsala, Sweden: BiacoreAB).

Bommakanti, G., Citron, M.P., Hepler, R.W., Callahan, C., Heidecker, G.J., Najar, T.A., Lu, X., Joyce, J.G., Shiver, J.W., Casimiro, D.R., et al. (2010). Design of an HA2-based *Escherichia coli* expressed influenza immunogen that protects mice from pathogenic challenge. Proc. Natl. Acad. Sci. U S A *107*, 13701–13706.

Burger, V.M., Vandervelde, A., Hendrix, J., Konijnenberg, A., Sobott, F., Loris, R., and Stultz, C.M. (2017). Hidden states within disordered regions of the CcdA antitoxin protein. J. Am. Chem. Soc. *139*, 2693–2701.

Chan, W.T., Espinosa, M., and Yeo, C.C. (2016). Keeping the wolves at bay: antitoxins of prokaryotic type II toxin-antitoxin systems. Front. Mol. Biosci. *3*, 9.

Christensen-Dalsgaard, M., and Gerdes, K. (2006). Two higBA loci in the *Vibrio cholerae* superintegron encode mRNA cleaving enzymes and can stabilize plasmids. Mol. Microbiol. *62*, 397–411.

Dao-Thi, M.H., Van Melderen, L., De Genst, E., Afif, H., Buts, L., Wyns, L., and Loris, R. (2005). Molecular basis of gyrase poisoning by the addiction toxin CcdB. J. Mol. Biol. *348*, 1091–1102.

Drobnak, I., De Jonge, N., Haesaerts, S., Vesnaver, G., Loris, R., and Lah, J. (2013). Energetic basis of uncoupling folding from binding for an intrinsically disordered protein. J. Am. Chem. Soc. *135*, 1288–1294.

Dutta, A., Krieger, J., Lee, J.Y., Garcia-Nafria, J., Greger, I.H., and Bahar, I. (2015). Cooperative dynamics of intact AMPA and NMDA glutamate receptors: similarities and subfamily-specific differences. Structure *23*, 1692–1704.

General, I.J., Liu, Y., Blackburn, M.E., Mao, W., Gierasch, L.M., and Bahar, I. (2014). ATPase subdomain IA is a mediator of interdomain allostery in Hsp70 molecular chaperones. PLoS Comput. Biol. *10*, e1003624.

Gerdes, K., and Maisonneuve, E. (2012). Bacterial persistence and toxin-antitoxin loci. Annu. Rev. Microbiol. *66*, 103–123.

Gerdes, K., Rasmussen, P.B., and Molin, S. (1986). Unique type of plasmid maintenance function: postsegregational killing of plasmid-free cells. Proc. Natl. Acad. Sci. U S A *83*, 3116–3120.

Gruszka, D.T., Mendonca, C.A., Paci, E., Whelan, F., Hawkhead, J., Potts, J.R., and Clarke, J. (2016). Disorder drives cooperative folding in a multidomain protein. Proc. Natl. Acad. Sci. U S A *113*, 11841–11846.

Gupta, K., Tripathi, A., Sahu, A., and Varadarajan, R. (2017). Contribution of the chromosomal ccdAB operon to bacterial drug tolerance. J. Bacteriol. *199*, JB.00397–17.

Hayes, F. (2003). Toxins-antitoxins: plasmid maintenance, programmed cell death, and cell cycle arrest. Science *301*, 1496–1499.

De Jonge, N., Garcia-Pino, A., Buts, L., Haesaerts, S., Charlier, D., Zangger, K., Wyns, L., De Greve, H., and Loris, R. (2009). Rejuvenation of CcdB-poisoned gyrase by an intrinsically disordered protein domain. Mol. Cell *35*, 154–163.

Kamar, R.I., Banigan, E.J., Erbas, A., Giuntoli, R.D., Olvera de la Cruz, M., Johnson, R.C., and Marko, J.F. (2017). Facilitated dissociation of transcription factors from single DNA binding sites. Proc. Natl. Acad. Sci. U S A *114*, E3251–E3257.

Kaspy, I., Rotem, E., Weiss, N., Ronin, I., Balaban, N.Q., and Glaser, G. (2013). HipA-mediated antibiotic persistence via phosphorylation of the glutamyl-tRNA-synthetase. Nat. Commun. *4*, 3001.

Li, H., Sharma, N., General, I.J., Schreiber, G., and Bahar, I. (2017). Dynamic modulation of binding affinity as a mechanism for regulating interferon signaling. J. Mol. Biol. *429*, 2571–2589.

Loris, R., Dao-Thi, M.H., Bahassi, E.M., Van Melderen, L., Poortmans, F., Liddington, R., Couturier, M., and Wyns, L. (1999). Crystal structure of CcdB, a topoisomerase poison from *E. coli*. J. Mol. Biol. *285*, 1667–1677.

Madl, T., Van Melderen, L., Mine, N., Respondek, M., Oberer, M., Keller, W., Khatai, L., and Zangger, K. (2006). Structural basis for nucleic acid and toxin recognition of the bacterial antitoxin CcdA. J. Mol. Biol. *364*, 170–185.

Maisonneuve, E., Shakespeare, L.J., Jorgensen, M.G., and Gerdes, K. (2011). Bacterial persistence by RNA endonucleases. Proc. Natl. Acad. Sci. U S A *108*, 13206–13211.

Maki, S., Takiguchi, S., Horiuchi, T., Sekimizu, K., and Miki, T. (1996). Partner switching mechanisms in inactivation and rejuvenation of *Escherichia coli* DNA gyrase by F plasmid proteins LetD (CcdB) and LetA (CcdA). J. Mol. Biol. *256*, 473–482.

Van Melderen, L., Bernard, P., and Couturier, M. (1994). Lon-dependent proteolysis of CcdA is the key control for activation of CcdB in plasmid-free segregant bacteria. Mol. Microbiol. *11*, 1151–1157.

Muthuramalingam, M., White, J.C., and Bourne, C.R. (2016). Toxin-antitoxin modules are pliable switches activated by multiple protease pathways. Toxins (Basel) *8*, toxins8070214.

Page, R., and Peti, W. (2016). Toxin-antitoxin systems in bacterial growth arrest and persistence. Nat. Chem. Biol. *12*, 208–214.

Pandey, D.P., and Gerdes, K. (2005). Toxin-antitoxin loci are highly abundant in free-living but lost from host-associated prokaryotes. Nucleic Acids Res. *33*, 966–976.

Pettersen, E.F., Goddard, T.D., Huang, C.C., Couch, G.S., Greenblatt, D.M., Meng, E.C., and Ferrin, T.E. (2004). UCSF Chimera—a visualization system for exploratory research and analysis. J. Comput. Chem. *25*, 1605–1612.

Ramisetty, B.C.M., and Santhosh, R.S. (2017). Endoribonuclease type II toxin-antitoxin systems: functional or selfish? Microbiology *163*, 931–939.

Rowe-Magnus, D.A., Guerout, A.M., Biskri, L., Bouige, P., and Mazel, D. (2003). Comparative analysis of superintegrons: engineering extensive genetic diversity in the Vibrionaceae. Genome Res. *13*, 428–442.

Sali, A., and Blundell, T.L. (1993). Comparative protein modelling by satisfaction of spatial restraints. J. Mol. Biol. *234*, 779–815.

Salmon, M.A., Van Melderen, L., Bernard, P., and Couturier, M. (1994). The antidote and autoregulatory functions of the F plasmid CcdA protein: a genetic and biochemical survey. Mol. Gen. Genet. *244*, 530–538.

Schreiber, G. (2017). The molecular basis for differential type I interferon signaling. J. Biol. Chem. *292*, 7285–7294.

Szekeres, S., Dauti, M., Wilde, C., Mazel, D., and Rowe-Magnus, D.A. (2007). Chromosomal toxin-antitoxin loci can diminish large-scale genome reductions in the absence of selection. Mol. Microbiol. *63*, 1588–1605.

Tripathi, A., Dewan, P.C., Barua, B., and Varadarajan, R. (2012). Additional role for the ccd operon of F-plasmid as a transmissible persistence factor. Proc. Natl. Acad. Sci. U S A *109*, 12497–12502.

Tripathi, A., Dewan, P.C., Siddique, S.A., and Varadarajan, R. (2014). MazF-induced growth inhibition and persister generation in *Escherichia coli*. J. Biol. Chem. *289*, 4191–4205.

Tripathi, A., Gupta, K., Khare, S., Jain, P.C., Patel, S., Kumar, P., Pulianmackal, A.J., Aghera, N., and Varadarajan, R. (2016). Molecular determinants of mutant phenotypes, inferred from saturation mutagenesis data. Mol. Biol. Evol. *33*, 2960–2975.

Tripathi, A., Swaroop, S., and Varadarajan, R. (2019). Molecular determinants of temperature-sensitive phenotypes. Biochemistry *58*, 1738–1750.

Wienken, C.J., Baaske, P., Rothbauer, U., Braun, D., and Duhr, S. (2010). Protein-binding assays in biological liquids using microscale thermophoresis. Nat. Commun. *1*, 100.

Wood, T.K. (2016). Combatting bacterial persister cells. Biotechnol. Bioeng. *113*, 476–483.

STAR★METHODS

KEY RESOURCES TABLE

REAGENT or RESOURCE	SOURCE	IDENTIFIER
Bacterial and Virus Strains		
BL21DE3* *E. coli*.	Thermo Fisher Scientific	Cat#EC0114
CSH501 *E. coli*.(Bajaj et al., 2005)	(Bajaj et al., 2005)	NA
Chemicals, Peptides, and Recombinant Proteins		
CcdA50-72-R57C	This paper	NA
E487C GyrA14	This paper	NA
Tetramethylrhodamine-5-Maleimide	Thermo Fisher Scientific	Cat#T6027
Fluorescein-5-Maleimide	Thermo Fisher Scientific	Cat#62245
CcdA45-72(Tripathi et al., 2016)	(Tripathi et al., 2016)	NA
NT-647-NHS dye	NanoTemper Technologies	Cat#MO-L011
Deposited data		
Crystal structure of CcdB	(Loris et al., 1999)	PDB ID: 3vub
Crystal structure of CcdB dimer in complex with one C-terminal CcdA domain	(De Jonge et al., 2009)	PDB ID: 3hpw
Crystal structure of CcdB-gyrase complex	(Dao-Thi et al., 2005)	PDB ID: 1x75
Oligonucleotides		
Forward primer: CAGATCGCGTGTCTGTTGCGTA	This paper	NA
Reverse primer: CAACAGACACGCGATCTGATCCA	This paper	NA
Recombinant DNA		
pET15bHisGyrA14 plasmid	This paper	NA
pET15bHis E487C GyrA14	This paper	NA
Software and Algorithms		
CONSURF server	(Ashkenazy et al., 2016)	https://consurf.tau.ac.il/
UCSF-Chimera for visualization	(Pettersen et al., 2004)	https://www.cgl.ucsf.edu/chimera/download.html
Prody software suite	(Bakan et al., 2011)	http://prody.csb.pitt.edu/
BIAEvaluation Software 3.1(BIAevaluation Software Handbook version 3.1)	(BIAevaluation Software Handbook version 3.1, 1997)	GE Healthcare (BR-1005-97)
GROMACS	(Berendsen et al., 1995)	http://www.gromacs.org/
Modeller v9.14	(Sali and Blundell, 1993)	https://salilab.org/modeller/

LEAD CONTACT AND MATERIALS AVAILABILITY

Further information and requests for resources and reagents should be directed to and will be fulfilled by the Lead Contact, Prof. Raghavan Varadarajan (varadar@iisc.ac.in)

Lead contact for the material availability: Prof. Raghavan Varadarajan (varadar@iisc.ac.in). All unique/stable reagents generated in this study are available from the Lead Contact without restriction.

EXPERIMENTAL MODEL AND SUBJECT DETAILS

BL21DE3* *E. coli* and CSH501 *E. coli* strains have been used for the studies. Both the transformed strains are grown at 37°C overnight in LB broth (HiMedia) containing 100 μg/ml ampicillin. Additional details are provided in the Method Details section.

METHOD DETAILS

Protein Expression, Purification and Labeling

The wt CcdB protein was heterologously expressed in the pBAD24 vector and purified from CSH501 *E. coli* from the pBAD vector that is resistant to the toxic action of CcdB A single colony was inoculated into LB medium containing 100 μg/mL ampicillin and grown at

37°C overnight. 1% of the primary inoculum was inoculated in two litres of secondary culture in LB media containing 100 μg/mL ampicillin and grown at 37°C for 3 hours. Induction was carried out with 0.2% arabinose and cells were then grown at 30°C for 6 hrs. After cell harvesting by centrifugation, pellet was resuspended in 1/10th volume ice-cold resuspension buffer (10 mM HEPES buffer, 10% glycerol, 1 mM EDTA, and 0.5 mM PMSF, pH 8.0). Cell lysis was carried out by sonication on ice, followed by centrifugation at 14000g. The protein was purified from the soluble fraction of the lysate by a affinity chromatography using immobilized CcdA peptide (residues 45-72). Protein was eluted with 0.2 M glycine, pH 2.5, and 1 mL fractions were collected in 1.5 mL tubes containing 400 μL of 1.5 M Tris, pH 8.8, to neutralize the protein solution on elution. Fractions containing pure protein were pooled and dialyzed against 10 mM HEPES, pH 7, and stored at −20°C. CcdB was lyophilized in 50 mM ammonium carbonate at pH 8 and stored at 4°C. The CcdA synthetic peptides were obtained from Genscript. Protein purity was confirmed using SDS-PAGE and mass spectrometry. Immobilization of the CcdA peptides on Biorad Affigel-15 and GyrA14 protein on Biorad Affigel-10 was done as per the manufacturer's instructions. The immobilization was carried out by incubating beads with the peptide/protein at pH 7.5, buffered using sodium bicarbonate buffer at 4°C for 18 hrs, and subsequent blocking by using 1mM ethanol amine (Baliga et al., 2016).

Construction of Cysteine Mutants in Gyrase

Site directed mutagenesis was carried out using partially overlapping primers to generate pET15bHis E487C GyrA14 mutant. Inverse PCR like reactions were performed by using 10ng of wildtype pET15bHisGyrA14 plasmid as template for 20 cycles. The amplicons were DpnI treated to digest the parent Wildtype template and transformed into DH5α electro- competent cells. Positive clones were confirmed by Sanger sequencing from Macrogen.

Forward and reverse primer sequences were CAGATCGCGTGTCTGTTGCGTA and CAACAGACACGCGATCTGATCCA for E487C.

Purification and Labeling of GyraseA14 Cysteine Mutants

Wildtype, his tagged GyrA14 was purified (Bajaj et al., 2008). The 487C Cysteine mutant of Gyrase (pET15bHisGYRE487C) was expressed in BL21DE3* *E. coli* strain, purified and labelled as explained below.

Induction was carried out at 20°C overnight by adding 1mM IPTG at 0.8 O.D. Culture was pelleted at 4°C, resuspended (resuspension buffer-50 mM Sodium phosphate buffer, 0.5 mM EDTA, 0.5 M Sucrose, 1mMDTT, 200 μM PMSF, pH=7.5) and sonicated for three cycles with 2s ON/ 7s OFF pulse. The supernatant was clarified from whole cell lysate by centrifuging at 14000 RPM for 30min at 4°C and incubated with pre-equilibrated Ni- NTA resin (Pre- equilibration buffer- 20mM sodium phosphate buffer, 0.5M NaCl, 1mMDTT, pH=7.5) for 2hrs at 4°C. Non- specific binding was removed with washes (wash buffer- 50mM Imidazole in 20mM sodium phosphate buffer, 0.5M NaCl, 1mMDTT pH=7.5). Protein-bound beads were re-equilibrated with conjugation buffer (20mM sodium phosphate buffer, 150mM NaCl, 0.5mM EDTA, pH=7.2) to remove the thiol-containing groups. Labeling was performed with a five fold excess of dye. 100mM stock of Fluorescein-5-maleimide was prepared in DMSO and the required amount was mixed in 5 column volumes of conjugation buffer and incubated with the re-equilibrated protein-bound Ni-NTA beads for overnight at 4°C. Excess unbound dye was washed off, labeled protein was eluted with elution buffer (500mM Imidazole in 20mM sodium phosphate buffer, 0.5M NaCl, 1mM DTT, pH=7.5). The elute was dialysed into

Rejuvenation Kinetic Studies

To perform the rejuvenation studies, fluorescein labeled GyrA14-E487C (GyrA14*) was mixed with CcdB in equimolar ratio and incubated for 1 hr at room temperature to form the CcdB-GyrA14* complex. The rejuvenation of GyrA14* was initiated by mixing it with TMR labelled $CcdA_{50\text{-}72}$-R57C ($CcdA_{50\text{-}72}$*) at a final concentration of 0.5 to 5 μM. The kinetics was measured by monitoring the fluorescence of the donor fluorophore on GyrA14*. Refer to Supplemental Information for additional details on FRET.

Equilibrium and Kinetic Fluorescence Studies

The spectral fluorescence measurements were carried out using a Fluoromax-3 spectrofluorometer (Horiba). The excitation wavelength was 490 nm with a bandwidth of 1 nm. Emission was collected with a 5 nm bandwidth using an integration time of 1 second with a data pitch of 1 nm. Time-dependent fluorescence measurements for the donor fluorophore were carried out using excitation at 490 nm and emission at 520 nm. Stopped-flow kinetic studies were monitored using SFM4 coupled to MOS450 optical system from Biologic. The dead time of mixing was 10.3 ms, where the excitation was set to 490 nm with a bandwidth of 2 nm, and emission was collected at 520 nm using a band-pass optical filter (Asahi Spectra).

Fluorescence Kinetic Data Analysis

The kinetic data obtained by monitoring FRET were analyzed to delineate the rejuvenation mechanism. All kinetic traces were globally fitted to different schemes (Figure 2E; See Discussion) to infer the mechanism. During the analysis, all the steps in each kinetic model were assumed to be reversible. Each kinetic model used to fit the data was defined in a MATLAB using a set of differential equations. The simulated kinetic traces for each model were generated by solving the differential equations using the *ode23s* function. The simulated traces were fitted to the experimental data by minimizing RMSD between them using function *fminsearchbnd*, using a tolerance value of 10^{-5}. The kinetic parameters were floated over a broad range to eliminate bias. The fluorescence intensities of the initial and final state were fixed, while intensities of all the intermediates were allowed to change and assumed to be lower than the initial and final state. The fitting was initiated from diverse initial parameters to ensure that the obtained parameters do not represent local minima. The transition from $CcdB_2$:$CcdA_1$ to $CcdB_2$:$CcdA_2$ was not considered in the fitting, as it is silent to

fluorescence change thus, it could not be observed in the experiment. Furthermore, it is kinetically very fast and hence anticipated to have no influence either on the obtained kinetic parameters or in model discrimination.

Structural Analysis

Coordinates of crystal structures of *E. coli* CcdB dimer (3vub, (Loris et al., 1999)), CcdB-CcdA complex (3hpw, (De Jonge et al., 2009)) and CcdB-gyrase complex (1x75, (Dao-Thi et al., 2005)) were obtained from the PDB (Berman et al., 2000). Missing residues in the structures were modelled either by using a suitable template or using the loopmodel module of Modeller v9.14 (Sali and Blundell, 1993). Final models were energy minimized using the GROMACS package (Berendsen et al., 1995).

Computational Analyses

To understand residue-level flexibility of CcdB in the free and CcdA or GyrA14-bound states, the global motions pertaining to CcdB were determined using anisotropic network model based normal mode analysis (ANM-NMA). Further, to evaluate the impact of single residue perturbation on CcdB-GyrA structure, perturbation response scanning (PRS) was performed using the Prody package (Bakan et al., 2011).

Normal Mode Analysis (NMA)

To understand residue-level flexibility of CcdB in the free, CcdA-bound and GyrA14-bound states, the global motions pertaining to CcdB were determined using the Anisotropic Network Model based Normal Mode Analysis (ANM-NMA). For network generation, a Cα- Cα distance cut-off of 15Å and default fixed spring constant was used. Normal modes were calculated using Prody package (Bakan et al., 2011). The number of modes accounting for 80% of the variance in flexibility were considered in calculation of the square fluctuations and cross-correlation. The obtained square fluctuations were scaled between 0 and 1 by dividing the individual value with the maximum fluctuation value.

Perturbation Response Scanning (PRS)

Perturbation response scanning (PRS) was performed using the Prody package (Bakan et al., 2011). PRS allows evaluation of the impact of a single residue perturbation on the protein structure. For the calculations, a protein structure is represented as a mass-spring system. The mass is represented by the Cα atoms of the residues and the network is generated by defining edges between the Cα atoms within a distance cut-off of 15 Å. The default spring constant was used. Each residue is perturbed one at a time, at least 1000 times, by exerting a force with random direction and unit magnitude, and the response of all other residues to such perturbations is recorded. The row and column averages of the resultant matrices help in identifying the effector or sensor residues. Residues that cause maximum displacement in the structure upon perturbation are termed as effector residues while the residues that respond maximally to several perturbations are termed as sensor residues.

Sequence Conservation Analysis for CcdB

Sequence homologues of CcdB toxin were identified through the CONSURF server using the HMMER search algorithm for 3 iterations (Ashkenazy et al., 2016). A total of 150 sequences that sample the list of homologues to query CcdB sequence were collected at a minimum sequence identity of 35%. The chosen homologues were non-redundant at a sequence identity of 90%. Many of these homologues are annotated as CcdB toxins in different organisms. A multiple sequence alignment of the sequences was performed by CONSURF using the MAFFT algorithm, and conserved residues were identified.

SPR Experiments

All SPR experiments were performed with a Biacore 3000 (Biacore, Uppsala, Sweden) optical biosensor at 25°C. GyrA14 was used for immobilization at 30 μL/min flow rate for 180s. 1000 resonance units of GyrA14 were attached by standard amine coupling to the surface of a research-grade CM5 chip. A sensor surface (without GyrA14) that had been activated and deactivated served as a negative control for each binding interaction. 50 nM of the WT CcdB and S12G-CcdB proteins were then run across each sensor surface in a 1X PBS (pH 7.4) containing 0.005% Tween surfactant. For these experiments, the SPR was done in co-inject mode, where the association was allowed for 100secs, followed by immediate dissociation with different concentrations of the $CcdA_{45\text{-}72}$. Both association and dissociation were measured at a flow rate of 30 μL/min. In all cases, the sensor surface was regenerated between binding reactions by one to two washes with 4 M $MgCl_2$ for 30 s at 30 μL/min. Each binding curve was corrected for nonspecific binding by subtraction of the signal obtained from the negative control flow cell. The kinetic parameters were obtained by fitting the data to a simple 1:1 Langmuir interaction model by using BIA EVALUATION 3.1 software. To monitor the effect of labeling of CcdA $peptide_{50\text{-}72}$ on rejuvenation process, 50 nM of WT CcdB was passed for 100 sec on a Gyrase immobilized chip followed by immediate dissociation with three different concentration of both labeled and unlabeled CcdA $peptide_{50\text{-}72.}$ The effect of labelling of E487C GyraseA14* on binding to CcdB was probed by SPR. CcdB protein was immobilized on the surface of a CM5 sensor, using 10 mM sodium acetate buffer, pH 3.5 at an injection rate of 2 μL/min at 25 °C. Surface density of the ligand was 200 RUs. Both the CcdB immobilized channel surface and a control channel surface were similarly NHS and EDC activated and blocked using 1M Ethanolamine, pH=8.5. Running buffer was 1XPBS, pH=7.4, 0.05% P20 surfactant; flow rate for binding was 30 μL/ min. All the studies were carried out at 25 °C using Biacore 3000 optical biosensor. The kinetic parameters were fitted to the 1:1 Langmuir interaction model using BIAevaluation 3.0 software.

QUANTIFICATION AND STATISTICAL ANALYSIS

Table 1: To determine the robustness of the parameters listed in Table 1, fitting was initiated from various initial parameters. The values flagged with the superscript 'a' had standard deviations higher than their mean values. All other values were highly robust showing standard deviations of less than 50% for multiple independent fittings.

Figure 7: The squared fluctuation values in Figure 3are normalized between 0 and 1 by dividing the individual value with maximum fluctuation value. The response from PRS analysis shown in Figures 4, 5, 6, and 7 is normalized by dividing each value by the response of the perturbed residue.

Figures S2 and S5 For MST, each experiment has been carried out twice, each time with two sets of capillaries (n=4) and the listed errors are the standard error derived from the values obtained for individual replicates. The SPR experiments in Figure S5 have been performed once at each concentration with four different concentrations of the protein and the listed error is the standard error derived from the values at multiple concentrations.

DATA AND CODE AVAILABILITY

This study did not generate any unique datasets or code. The data relevant to the figures in the paper have been made available in the Supplemental Information.

Structure, Volume *28*

Supplemental Information

Mechanism of CcdA-Mediated Rejuvenation of DNA Gyrase

Nilesh K. Aghera, Jyothi Prabha, Himani Tandon, Gopinath Chattopadhyay, Sneha Vishwanath, Narayanaswamy Srinivasan, and Raghavan Varadarajan

Supplementary Information

Supporting tables:

Table S1: Interactions of CcdB residues with CcdA based on PDB structure 3G7Z which has two chains of CcdA bound to CcdB dimer. ΔASA is the difference between the solvent accessible surface area of the CcdB residues in free form (3VUB) and CcdA-bound form (3G7Z) (related to Figure 1).

CcdB Chain A	CcdA Interacting chain & residue no.	ΔASA - All atom (Å^2)	CcdB Chain B	CcdA Interacting chain & residue no.	ΔASA - All atom (Å^2)
8	D70, D,72	38.9	8	D65, D68, D69	27.1
			10	D68, D69	55.5
12	D72	31.5	12	D68	14.5
13	C58, D72	151.4	13	D62	101.8
14	C58, C59, D72	28.6	14	D58, D59, D65, D63	20.8
			17	D65	0.6
23	D45	20	23	C45	22.2
24	D41, D44, D45	85.7	24	C41, C44 C45	102.6
25	D44, D45, D52	22.8	25	C44, C45, C52	22.3
26	D45, D52	47.7	26	C52	69.9
27	D52	0.7	27	C52	4.1
28	D52, D53, D56	51.3	28	C52, C56	32
30	D64, D66, D67	42.6	30	D69, D71	54.3
35	D72	10.9	35	D65	10.9
37	C58	2.6	37	D58	1.3
41	C54, C58	63	41	D54, D58	56.8
42	C54, C55, C58	58	42	D54, D55, D58	64.3
43	C54	8.4	43	D54	5.5
45	C48, C50, C51	98	45	D48, D50, D51, D54	102.4
46	C51, C54, C55	57.5	46	D51, D54, D55	56.5
47	C44, C48	37.3	47	D44, D48	34.1
49	C44, C48	7			
50	C44, C52	15.8	50	D44, D52	15.8
51	C52, C55	30	51	D52, D55	29.5
64	C55, C58, C59	34.2	64	D55, D58, D59	33.9
66	C52, C55	1.1	66	D52, D55	0.6
67	C59, D71, D72	36.7	67	D59, D63, D65, D66	34.1
69	D70, D72	28.5	69	D65, D66, D69	26
70	D66, D70	12.7	70	D69, D71	16.7

71	D70, D72	16	71	D65, D69	16
			72	D69, D71	14.2
96	C44	41	96	D44	43
101	C40, C41, C44	92.5			

Table S2: Interactions of CcdA residues with CcdB based on PDB structure 3G7Z. ΔASA is the difference between solvent accessible surface area of the CcdA residues in the (fictitious) free form (removing CcdB from CcdBA complex) and CcdA-bound form (3G7Z) (related to Figure 1).

CcdA Chain C	**CcdB Interacting chain & residue no.**	**ΔASA - All atom (Å^2)**	**CcdA Chain D**	**CcdB Interacting chain & residue no.**	**ΔASA - All atom (Å^2)**
40	A101	17.6	40		
41	A101, B24	35.4	41	A24	37.6
44	A47, A49, A50, A96, A101, B24, B25	100.3	44	B47, B50, B96, A24, A25	133
45	B23, B24, B25	80.3	45	A23, A24, A25, A26	60
48	A47, A49	27.9	48	B47	34.8
50	A45	16	50	B45	33.3
51	A45, A46,	33.3	51	B45, B46	32.8
52	A50, A51, A66, B25, B26, B27, B28	105.4	52	B50, B51, B66, A26, A27, A28	106
53			53	A28	
54	A41, A42, A43, A46	71.6	54	B41, B42, B43, B45, B46	77.6
55	A42, A46, A51, A64, A66	80.7	55	B42, B46, B51, B64, B66	69.1
56	B28	32.1	56	A28	31.1
58	A13, A14, A37, A41, A42, A64,	76.9	58	B14, B37, B41, B42, B46, B64	97
59	A14, A64, A67	15.3	59	B14, B64, B67	39.9
			62	B13	10.1
			63	B14, B67	17.2
			64	A30	20.3
			65	B8, B17, B35, B67, B69, B71	162.6
			66	B67, B69, A70	64.8
			67	A30	27.9
			68	B8, B10, B12	48.6
			69	B8, B10, B30, B69, B70, B71, B72	71.1
			70	A8, A69, A70, A71	86.6
			71	B30, B70, B72	34.4

			72	A8, A12, A14, A35, A67, A69, A70, A71	211.6

Table S3: Interactions of CcdB residues with GyrA14 based on PDB structure 1X75. ΔASA is the difference between the solvent accessible surface area of the CcdB residues in free form (3VUB) and GyrA14-bound form (1X75) (related to Figure 1).

Chain C of CcdB	**GyrA interacting chain and residue no.**	**ΔASA – All atom (Å²)**	**Chain D of CcdB**	**GyrA interacting chain and residue no.**	**ΔASA - All atom (Å²)**
24	A375, A376, A379	76.4	24	B375, B376, B379	87.8
25	A376	3.4	25	B376	6
26	A368, A372	35.5	26	B368	30.9
87	A407, A456, A460	37.9	87	B407, B456, B460	34.9
88	A403, A456, A460, B464	53.2	88	B403, B456, B460, A464	53.7
91	B462	58.6	91	A462, B456, B460	54.6
92	B462, B464, B465	33.5	92	A462, A464, A465	25.5
95	A462, B462	36	95	A462, B462	34.1
96	B376	31.7	96	A376	32.4
99	A462, B460, B462	38.9	99	A460, A462, B462	35.5
100	B376	7.5	100	A376	7.5
101	B379, B380, B383, B457, B474	176.8	101	A379, A380, A383, A457, A461, A474,	170.5

Table S4: Interactions of GyrA14 residues with CcdB based on PDB structure 1X75. ΔASA is the difference between the solvent accessible surface area of the GyrA14 residues in the free form obtained after removing CcdB from 1X75 and GyrA14-bound form (1X75) (related to Figure 1).

Chain A of GyrA	**CcdB interacting chain and residue no**	**ΔASA – All atom (Å²)**	**Chain B of GyrA**	**CcdB interacting chain and residue no**	**ΔASA -All atom (Å²)**
368	C26	20.1	368	D26	16
372	C26				
375	C24	18.2	375	D24	15
376	C24, C25, D96, D100	98	376	D24, D25, C96, C100	97.5
379	C24, D101	29.7	379	D24, C101	34.8
380	D101	7.8	380	C101	9.2
383	D101	16.1	383	C101	16.4
403	C88	14	403	D88	15.5
407	C87	9.2	407	D87	8.6
456	C87, C88	53.5	456	D87, D88, D91	62.3
457	D101	7.2	457	C101	7
460	C87, C88, D91, D92, D95, D99	42.4	460	C99, D87, D88, D91	43.
461	D101	8.8			
462	C95, C99, D91, D92, D95 D99	99.2	462	C91, C92, C95, C99, D95, D99	77.9
464	D88, D92	30.9	464	C88, C92	21.5
465	D92	40	465	C92	26.9

Supporting figures:

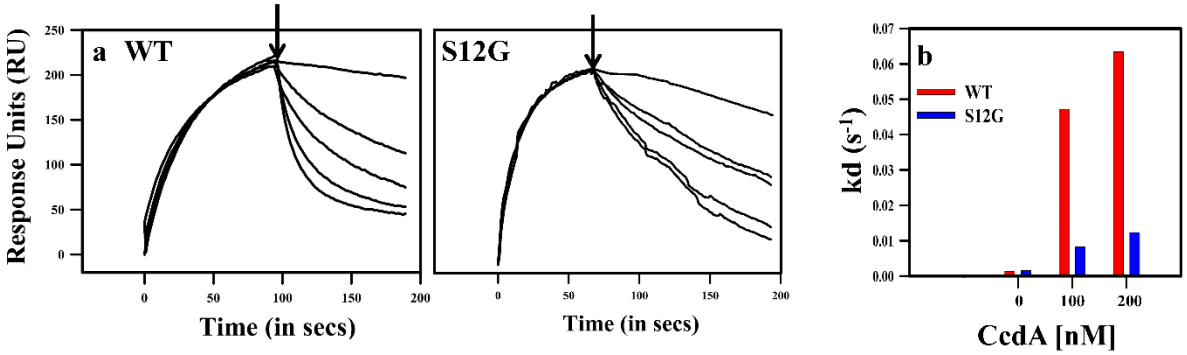

Figure S1: Dissociation of CcdB from GyrA14 in presence and absence of $CcdA_{45-72}$ (related to Figures 4 and 5). Overlays show the binding kinetics of 50 nM CcdB which is passed over Gyrase A immobilized on a CM5 chip for 100secs followed by dissociation mediated by different concentrations of $CcdA_{45-72}$. The arrow (↓) indicates the time of addition of CcdA. (a) Overlays show the dissociation of WT CcdB (left) bound to Gyrase with CcdA peptide, concentration increasing from the top to bottom (0 nM, 10 nM, 25 nM, 100 nM, 200 nM) and dissociation of S12G (right) bound to Gyrase with CcdA peptide, concentration increasing from the top to bottom (0 nM, 100 nM, 200 nM, 1000 nM, 5000 nM). The ligand GyrA14 was immobilized on the CM5 chip by standard amine coupling. (b) The apparent dissociation rate constants (kd) mediated by $CcdA_{45-72}$ are approximately five-fold lower for the S12G-CcdB-GyraseA14 complex than for WT-CcdB-GyraseA14.

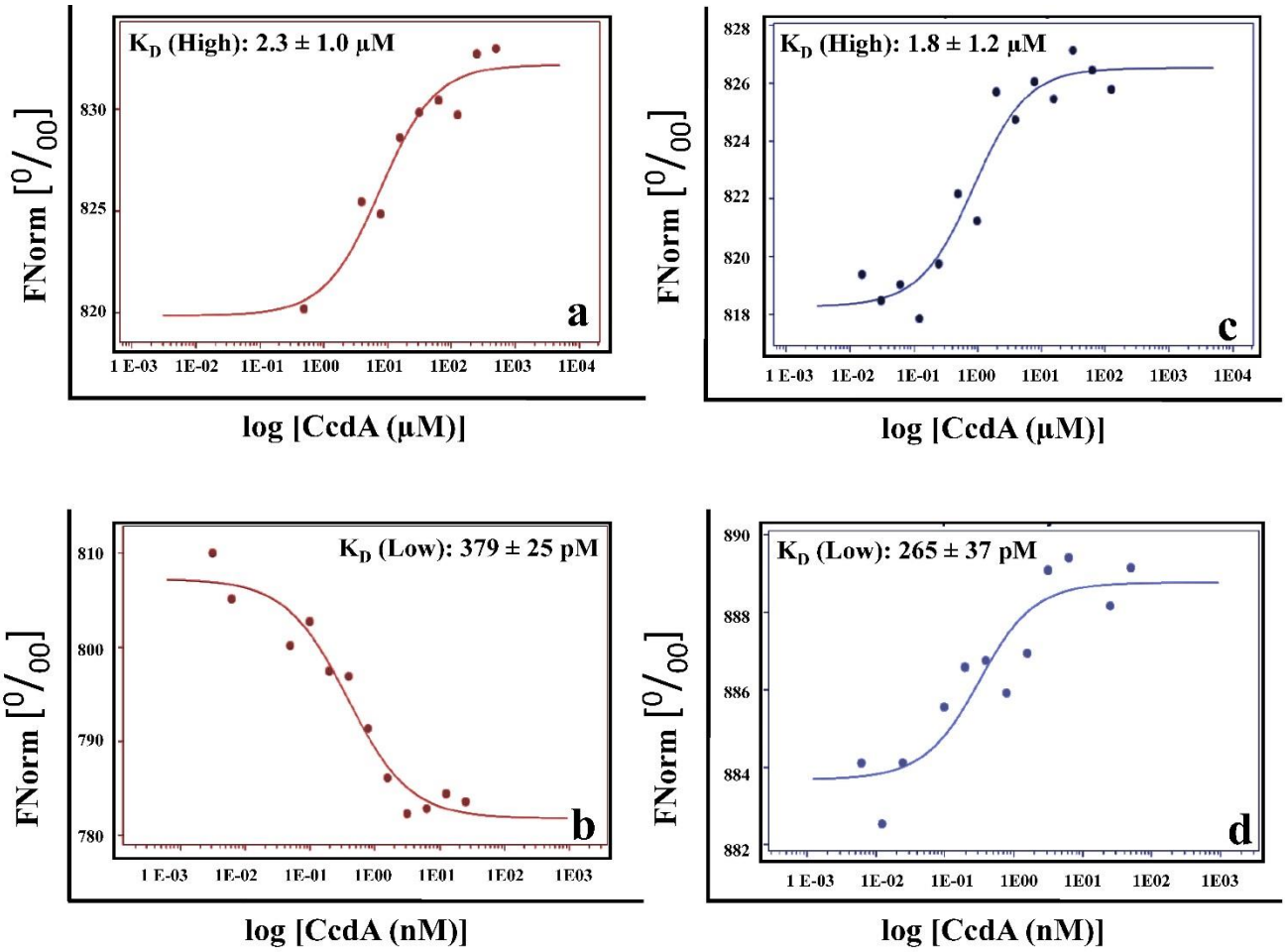

Figure S2: CcdB WT and S12G CcdB have similar affinity for CcdA$_{45\text{-}72}$ as determined by MicroScale Thermophoresis (related to Figures 4 and 5). CcdB WT (red) and S12G (blue) were labeled with Monolith™ Protein Labeling Kit NT-647-NHS dye (NanoTemper Technologies) according to the manufacturer's instructions, used at a concentration of 110 nM and titrated with two different concentration ranges of CcdA$_{45\text{-}72}$ to determine the K_D for both the high and low affinity binding sites for CcdB WT (a-b) and S12G (c-d). All studies were carried out in 200 mM HEPES, pH 8.4 and at 27 °C. The normalised fluorescence FNorm is plotted as parts per thousand [‰] as a function of [CcdB]. For each capillary (each measuring point), an MST trace is recorded. All traces are then normalised to start at 1000. For each trace, the FNorm value for the dose- response curve is calculated by dividing Fhot (MST laser on)/Fcold (MST laser off). The dissociation constants (K_D) were determined employing standard data analysis with MO.Affinity Analysis Software (Wienken *et al*, 2010).

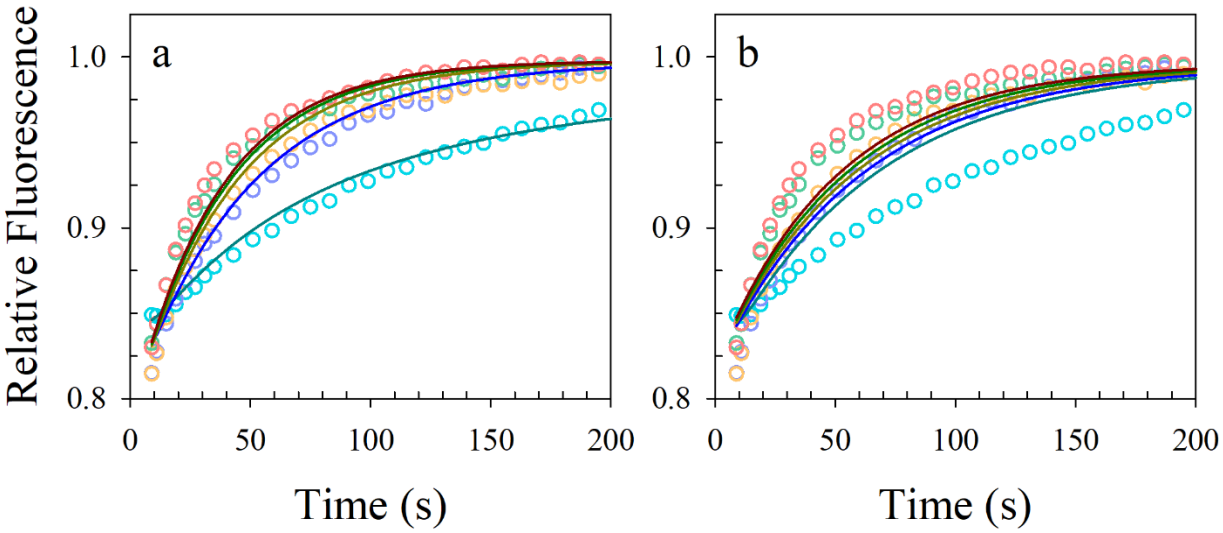

Figure S3: Global analysis of the rejuvenation data with single pathway (related to Figure 2). Panels a and b show global fitting to the concentration dependent rejuvenation traces using scheme 1 assuming $\lambda_4 << \lambda_3$ and $\lambda_2 << \lambda_4$, respectively. λ represents the kinetic flux through a given step, whereas k represents the corresponding microscopic rate constant.

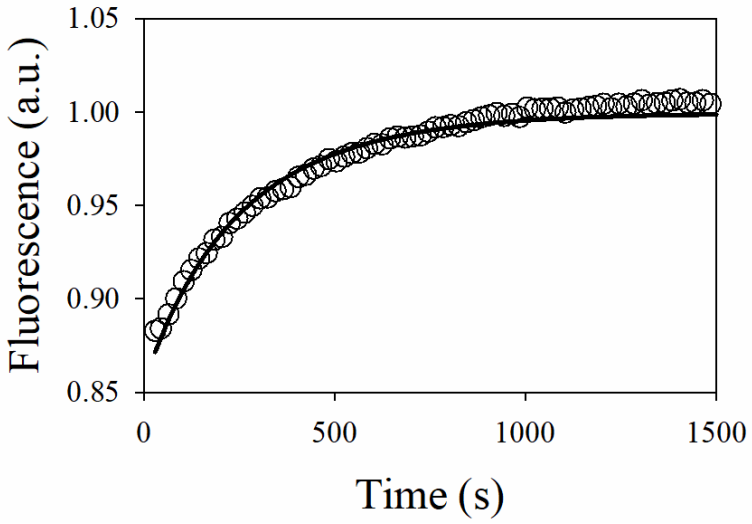

Figure S4: Rejuvenation using sub-stochiometric fraction of CcdA* (related to Figure 2). Rejuvenation trace acquired upon mixing CcdB-GyrA14* complex with CcdA* in 2:1 ratio. The rejuvenation process slows down by about fivefold with a twofold decrease in CcdA* concentration. This validates the requirement for two pathways in the rejuvenation process in scheme 1. The solid line represents fit to the data using scheme 1.

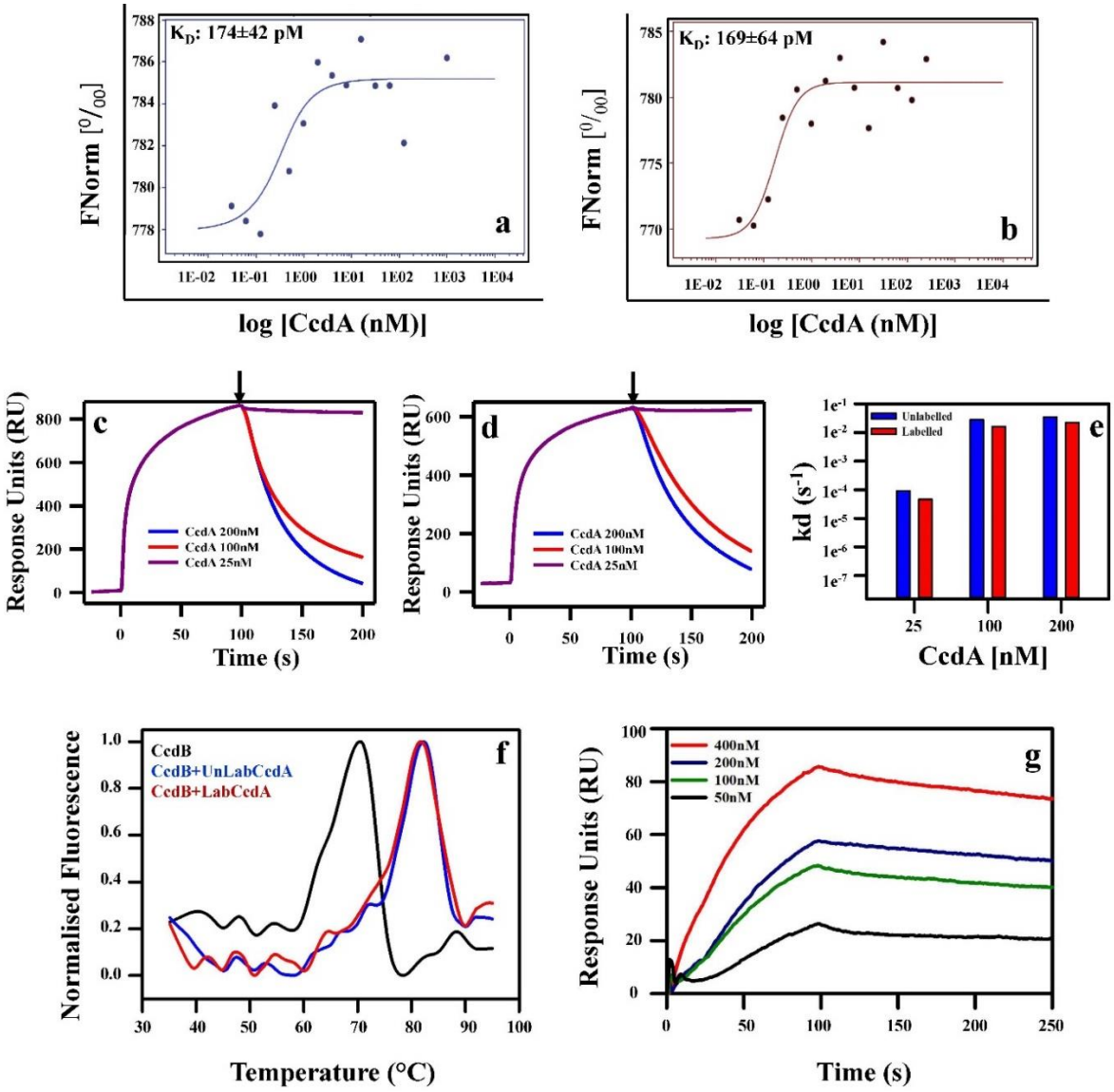

Figure S5: Both unlabelled and labelled $CcdA_{50\text{-}72}$ and Gyrase have similar affinity for CcdB WT as determined by MicroScale Thermophoresis, SPR and Tycho and SPR respectively (related to Figure 2). CcdB WT was labeled with Monolith™ Protein Labeling Kit NT-647-NHS dye (NanoTemper Technologies) according to the manufacturer's instructions, used at a concentration of 3 nM and titrated with different concentration ranges of (a) unlabelled $CcdA_{50\text{-}72}$ and (b) labelled $CcdA_{50\text{-}72}$ to determine the K_D for CcdB WT. All studies were carried out in 1XPBS, pH 7.4 and at 25 °C. The normalised fluorescence FNorm is plotted as parts per thousand [$^0/_{00}$] as a function of [CcdA]. For each capillary (each measuring point), an MST trace is recorded. All traces are then normalised to start at 1000. For each trace, the FNorm value for the dose-response curve is calculated by dividing Fhot (MST laser on)/Fcold (MST laser off). The dissociation constants (K_D) were determined employing standard data analysis with MO. Affinity Analysis Software (Wienken et al., 2010). (c-d) Overlays show the binding kinetics of 50 nM CcdB which is passed over Gyrase A immobilized on a CM5 chip for 100secs followed by dissociation

mediated by different concentrations of (c) unlabelled $CcdA_{50\text{-}72}$ and (d) labelled $CcdA_{50\text{-}72}$. The arrow (↓) indicates the time of addition of CcdA. Overlays show the dissociation of WT CcdB bound to Gyrase with unlabelled CcdA peptide (left), concentration increasing from the top to bottom (25 nM, 100 nM, 200 nM) and with labelled CcdA peptide (right), concentration increasing from the top to bottom (25 nM, 100 nM, 200 nM). The ligand GyrA14 was immobilized on the CM5 chip by standard amine coupling. (e) The apparent dissociation rate constants (kd) mediated by both unlabelled and labelled $CcdA_{50\text{-}72}$ are similar for the CcdB-GyraseA14 complex. (f) Thermal unfolding experiment of CcdB WT as well as complex with unlabelled $CcdA_{50\text{-}72}$ (blue) and labelled $CcdA_{50\text{-}72}$ (red) were carried out by nanoTemper Tycho (Tycho NT.6) by applying a thermal ramp of 30°C/min. 10µL of each CcdB protein (2 µM) with or without 5 µM of unlabelled and labelled $CcdA_{50\text{-}72}$ was subjected to thermal unfolding. (g) Binding sensogram of fluorescein labeled E487CGyrA14 (E487CGyrA14*) with CcdB, monitored by SPR on Biacore3000. Different concentrations of E487CGyrA14* mutant (50, 100, 200, and 400 nM from bottom to top), when passed as analytes over CcdB immobilized sensor channel surface, showed similar binding with CcdB. The E487CGyrA14* mutant binds with a K_D of 22 ± 10 nM with a k_{on} of 0.8 $\times 10^5$ ± 0.15 × 10^5 $M^{-1}s^{-1}$and a k_{off} of 1.46 × 10^{-3} ± 0.4 × 10^{-3} s^{-1}at 25 °C, similar to that previously reported for WT GyrA14 which binds with a k_{on} of 1.4×10^5 $M^{-1}s^{-1}$, a k_{off} of 1.3 × 10^{-3} s^{-1} and a K_D of 9.4 nM (Tripathi et al., 2019).